targets

MDPI

Review

Recent Progress in Small Molecule Fluorescent Probes for Imaging and Diagnosis of Liver Injury

Shuo Liu [1,2], Fei Huang [2], Xinyi Huang [1,3,*], Fuxin Zhang [2], Dong Pei [2], Jinlong Zhang [2] and Jun Hai [2,*]

[1] College of Science, Gansu Agricultural University, Lanzhou 730070, China; 1073323120453@st.gsau.edu.cn
[2] CAS Key Laboratory of Chemistry of Northwestern Plant Resources, Key Laboratory for Natural Medicine of Gansu Province, Lanzhou Institute of Chemical Physics, Chinese Academy of Sciences (CAS), Lanzhou 730070, China; h15628982782@163.com (F.H.); zhangfuxin@licp.cas.cn (F.Z.); dongpei@licp.cas.cn (D.P.); zhangjinlong@licp.cas.cn (J.Z.)
[3] Key Laboratory of Chemistry in Ethnic Medicinal Resources, State Ethnic Affairs Commission & Ministry of Education, Yunnan Minzu University, Kunming 650500, China
* Correspondence: huangxy@ymu.edu.cn (X.H.); haijun@licp.cas.cn (J.H.)

Abstract: The liver is an essential metabolic organ that is involved in energy metabolism, protein synthesis, and detoxification. Many endogenous and exogenous factors can cause liver injury, a complex pathological condition. It poses a serious risk to human health due to its extremely varied clinical manifestations, which range from mild fatty liver to liver fibrosis, cirrhosis, and even hepatocellular carcinoma. Because of their low specificity, lack of real-time monitoring, and invasiveness, traditional diagnostic techniques for liver injury, such as histopathological examination and serological analysis, have inherent limitations. Fluorescent probe technology, which offers high sensitivity, non-invasiveness, and real-time imaging capabilities, has become a potent tool in liver injury research and early diagnosis in recent years. The pathophysiology of liver injuries caused by alcohol, chemicals, drugs, and the immune system is methodically covered in this review, along with new developments in fluorescent probe development for their detection. The focused imaging properties of various fluorescent probes are highlighted, along with their possible uses in drug screening and early liver injury detection. This review attempts to offer theoretical insights to support the optimization of precision diagnostic and therapeutic approaches by summarizing these findings.

Keywords: fluorescent probe; liver injury; small molecule; fluorescence imaging

check for updates

Academic Editor: Jinbin Liu

Received: 11 April 2025
Revised: 12 May 2025
Accepted: 20 May 2025
Published: 28 May 2025

Citation: Liu, S.; Huang, F.; Huang, X.; Zhang, F.; Pei, D.; Zhang, J.; Hai, J. Recent Progress in Small Molecule Fluorescent Probes for Imaging and Diagnosis of Liver Injury. *Targets* **2025**, *3*, 18. https://doi.org/10.3390/targets3020018

Copyright: © 2025 by the authors. Licensee MDPI, Basel, Switzerland. This article is an open access article distributed under the terms and conditions of the Creative Commons Attribution (CC BY) license (https://creativecommons.org/licenses/by/4.0/).

1. Introduction

The liver is an extremely intricate and multipurpose organ that is essential to many physiological functions, such as protein secretion, detoxification, glycogen storage, anabolism, excretion, and the recycling of vital nutrients [1]. A serious risk to human health, liver injury is one of the most prevalent conditions seen in clinical practice. The liver is especially susceptible to a variety of endogenous and exogenous pathogenic factors, which can cause a variety of liver diseases, because of its abundant blood supply and vital role in metabolic processes [2]. A major challenge in current medical research is the prevention and treatment of liver injury, which is a common pathological outcome of many liver disorders [3]. It can be caused by multiple factors, including alcoholic fatty liver disease, viral hepatitis, autoimmune hepatitis, and chemically induced liver damage [4]. These conditions may lead to inflammation, abnormal wound healing responses, and impaired liver function.

Based on the underlying causes, liver injury can be classified into two main categories: exogenous (e.g., alcohol, chemical toxins) and endogenous (e.g., metabolic disorders, immune dysfunction). Liver injury often manifests as hepatocyte necrosis and apoptosis, liver dysfunction, inflammatory responses, and structural alterations such as fibrosis [5]. Clinically, mild liver injury is typically reflected by abnormal liver enzyme levels, including AST and ALT, whereas severe liver damage may lead to coagulopathy, hepatic encephalopathy, and even multiple organ failure [6,7]. Furthermore, based on disease progression, liver injury can be categorized as ALI or CLI, each exhibiting distinct pathophysiological mechanisms and clinical outcomes [8].

Early diagnosis is critical for timely intervention and the preservation of liver function. However, traditional diagnostic methods have inherent limitations in detecting liver injury at an early stage. Serological testing, the most commonly used approach to assess liver function, primarily measures serum enzyme activity but is susceptible to external interferences [9]. Additionally, histopathological examination provides valuable diagnostic information but has a lag in detection and cannot dynamically monitor liver function in real time. Therefore, there is an urgent need for efficient and accurate diagnostic techniques to enable the early detection of liver injury.

In recent years, fluorescence imaging technology has emerged as a promising diagnostic tool in modern medical research due to its high sensitivity, real-time imaging capabilities, and ease of use [10]. Direct optical imaging using fluorescent probes targeting disease-related biomarkers (such as ROS, CYP450, and HClO) offers a valuable complement to traditional imaging techniques [11]. Over the past decade, numerous fluorescent sensors have been developed for rapid detection and in situ visualization of key biomolecules in vivo [12]. Meanwhile, there has been some literature summarizing and exploring the application of fluorescent probes in a certain type of liver injury disease or a certain type of biomarker related to the disease [13,14].

Given this background, this review systematically explores the pathological mechanisms underlying alcoholic, drug-induced, chemical, and immune-mediated liver injury, with a particular focus on the application and imaging capabilities of small-molecule fluorescent probes in a variety of liver injury models, excluding systems based on other technologies such as quantum dots or chemiluminescence. By summarizing recent advancements, this study aims to provide a theoretical foundation for the future design of fluorescent probes and their potential role in the precise diagnosis and treatment of liver diseases.

2. Alcoholic Liver Injury

2.1. Establishment of Alcoholic Liver Injury Models

ALI is a dynamic pathological process resulting from alcohol-induced hepatic dysfunction. Based on disease duration, ALI can be classified into acute ALI and chronic ALI. Acute ALI refers to sudden liver damage caused by excessive alcohol consumption within a short period. It is characterized by direct alcohol toxicity, significant inflammatory activation, hepatocellular necrosis, inflammatory infiltration, and a sharp decline in liver function. In severe cases, acute liver failure may occur, posing a life-threatening risk to patients [15]. In contrast, chronic ALI results from long-term, continuous, or recurrent alcohol consumption. With prolonged alcohol metabolism, ROS accumulate, while hepatic antioxidant capacity declines, leading to fatty degeneration, chronic inflammation, and hepatic fibrosis. If left untreated, chronic ALI may progress to alcoholic hepatitis, cirrhosis, or even hepatocellular carcinoma.

Upon alcohol ingestion, most of it is absorbed in the intestines and transported to the liver for metabolism via the bloodstream. Alcohol dehydrogenase and acetaldehyde

dehydrogenase sequentially convert ethanol into acetaldehyde and acetic acid, which are ultimately metabolized into water and carbon dioxide via the tricarboxylic acid cycle [16,17]. However, prolonged and excessive alcohol consumption inhibits adenosine monophosphate-activated protein kinase, leading to hepatic triglyceride and cholesterol accumulation, thereby contributing to alcoholic fatty liver. Furthermore, excessive ethanol metabolism generates acetaldehyde, a cytotoxic metabolite that damages hepatocyte membranes, activates immune responses, and induces the production of ROS, exacerbating oxidative stress injury [18–20]. Additionally, alcohol metabolites activate Kupffer cells, stimulating the secretion of pro-inflammatory cytokines such as TNF-α, which further promotes hepatocyte apoptosis and leads to hepatic necrosis [21–23].

To simulate acute ALI in animal models (Figure 1), Yang et al. administered 12 mL/kg per day of 52° liquor via intragastric gavage in mice. After 14 days, a preliminary acute ALI model was successfully established [24]. Similarly, Zheng et al. induced acute liver injury in C57BL/6 mice by a single injection of 12 mL/kg of 50° white wine [25].

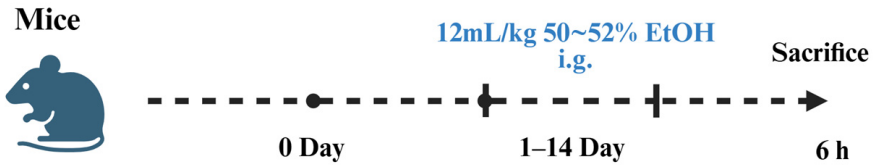


Figure 1. Schematic Representation of Animal Models for ALI.

Additionally, introducing dietary interventions such as high-fat and high-fructose diets during alcohol exposure significantly aggravates ALI severity, a phenomenon referred to as the "two-hit" model [26,27].

These experimental models are simple, cost-effective, and highly reproducible, with short induction periods, low mortality rates, and high stability. Furthermore, these models closely mimic alcohol-induced hepatic damage in humans, making them ideal tools for studying the pathogenesis and potential therapeutic strategies for acute ALI. Meanwhile a large number of fluorescent probes for the detection of ALI already exist (Table 1).

Table 1. Characterization of fluorescent probes in the ALI model.

Compounds	Trigger	λex (nm)	λem (nm)	Ref.
ICQ	Viscosity	630	740	[28]
MSOT	CYP450	710	750	[29]
DCI-Ac-Cys	Cys	540	705	[30]
BDP-ENE-Fur-HClO	HClO	620	700	[31]
HOTPy	viscosity	548	614	[32]
PPBI	Viscosity Polarity	575 400	750 497	[33]
WTH	HClO H_2O_2	440 360	500/605 450/605	[34]
BDP-NIR-ONOO	$ONOO^-$	920	700	[35]
Cy-ND	Viscosity	766	806	[36]
WZ-HOCl	HOCl	460	560	[37]

2.2. Application of Fluorescent Probes in Alcoholic Liver Injury

Feng et al. developed three mitochondria-targeted and viscosity-sensitive fluorescent probes (ICR, ICJ, and ICQ) for detecting AALI (Figure 2A). Among them, ICQ exhibits near-

infrared fluorescence, a large Stokes shift, and high viscosity sensitivity. ICQ specifically targets mitochondria, enabling the sensitive tracking of mitochondrial viscosity changes. In vivo, ICQ localizes to the liver and facilitates noninvasive, real-time imaging of liver viscosity alterations. Using these properties, ICQ has been successfully applied to visualizing AALI progression, revealing a significant increase in viscosity during liver injury. This study provides a sensitive and noninvasive method for AALI detection and demonstrates the potential of mitochondrial viscosity as a biomarker for AALI [28].

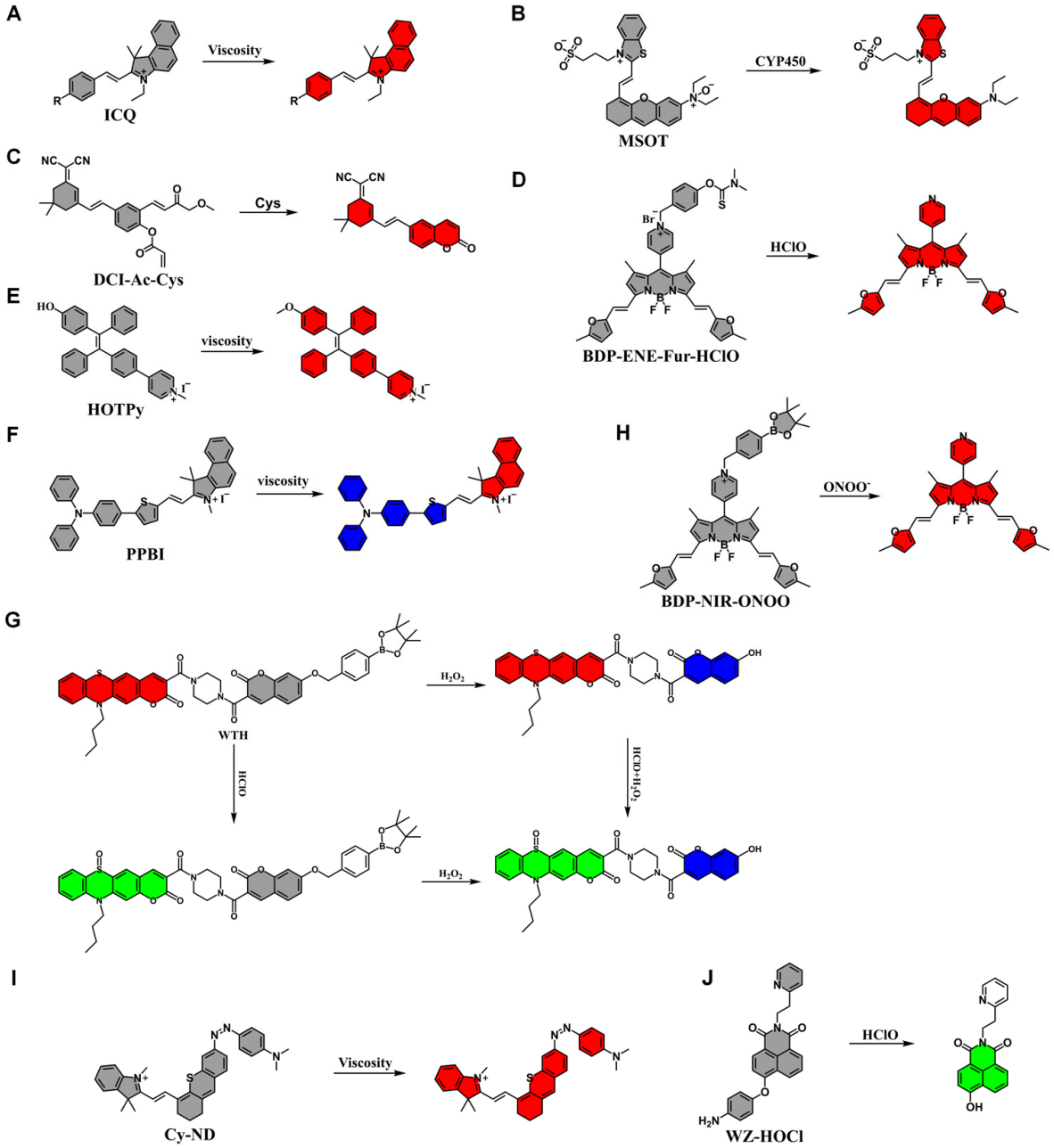


Figure 2. (**A**–**J**) Structure and detection mechanism of fluorescent probe in ALI models.

Wu et al. designed a water-soluble activatable fluorescent probe for imaging ALI using near-infrared fluorescence and multispectral optoacoustic tomography (MSOT) (Figure 2B). The probe is activated in situ in response to CYP450 reductase overexpression under hypoxic liver conditions, converting an N-oxide moiety into an aromatic tertiary amine, leading to enhanced fluorescence and red-shifted absorption. This activation generates both fluorescence and photoacoustic signals, enabling real-time imaging and monitoring of ALI

progression and recovery in mouse models. Moreover, MSOT imaging precisely localizes liver damage, providing an essential tool for studying pathophysiological processes in ALI. This work highlights the potential of MSOT and fluorescence imaging in biomedical research [29].

Yang et al. developed a near-infrared fluorescent probe, DCI-Ac-Cys, which undergoes a Cys-triggered cascade reaction to form a coumarin fluorophore (Figure 2C). The acrylate-based DCI-Ac-Cys probe exhibits high selectivity for Cys, eliminating interference from other biothiols. Using DCI-Ac-Cys, researchers successfully achieved sensitive imaging of intracellular Cys and constructed cellular and mouse models of ALI. Additionally, the probe was applied to evaluate the therapeutic efficacy of antioxidant drugs (silybin and curcumin) in ALI treatment. These findings suggest that Cys may serve as a potential biomarker for ALD and introduce a novel method for ALD drug screening and diagnostic evaluation [30].

Zhang et al. developed a near-infrared fluorescent probe (BDP-ENE-Fur-HClO) capable of detecting HClO, enabling real-time imaging of ALD (Figure 2D). The probe demonstrated high sensitivity, selectivity, rapid detection, and near-infrared emission for in vitro HClO detection. It effectively tracked endogenous/exogenous HClO in living cells without interference from other ROS and was successfully applied in ALD cell models. Furthermore, BDP-ENE-Fur-HClO monitored exogenous HClO in normal mice and highly expressed HClO in peritonitis mice, enabling inflammation diagnosis and the evaluation of ALD drug treatments. This work provides a powerful tool for ALD diagnosis [31].

Chen et al. synthesized an AIE fluorescent probe (HOTPy) with pyridine and hydroxyl functional groups to enhance water solubility and chemical stability (Figure 2E). The probe exhibits high sensitivity and selectivity for viscosity detection, along with excellent biocompatibility and precise mitochondrial localization. Using live-cell imaging, HOTPy effectively sensed viscosity changes in ALI models. Additionally, HOTPy was successfully applied to in vivo imaging of AALI mice, allowing for real-time monitoring of liver viscosity fluctuations and tracking drug intervention effects. This study provides a novel AIE probe for the diagnosis and management of viscosity-related liver diseases [32].

Yu et al. have developed a novel dual-responsive fluorescent probe, PPBI, which simultaneously responds to polarity and viscosity (Figure 2F). By incorporating a positively charged half-carbonyl main chain into triphenylamine derivatives, PPBI exhibits deep red fluorescence along with AIE properties (Figure 3). The probe demonstrates excellent biocompatibility and can be used to precisely localize mitochondria and lipid droplets in live cells. Furthermore, it enables the distinction between cancerous and normal cells through fluorescence changes in both green and red channels. PPBI is also capable of monitoring abnormal fluctuations in intracellular viscosity and polarity linked to inflammation and ferroptosis. Notably, in a mouse model, in vivo imaging amplified these changes in polarity and viscosity, allowing for the monitoring of AALI and tracking the healing process of the damaged liver under drug intervention. This provides a powerful visual tool for both diagnosing and treating AALI. Overall, PPBI holds great promise as a tool for studying diseases related to biological polarity and viscosity, as well as for bioimaging and medical diagnostics [33].

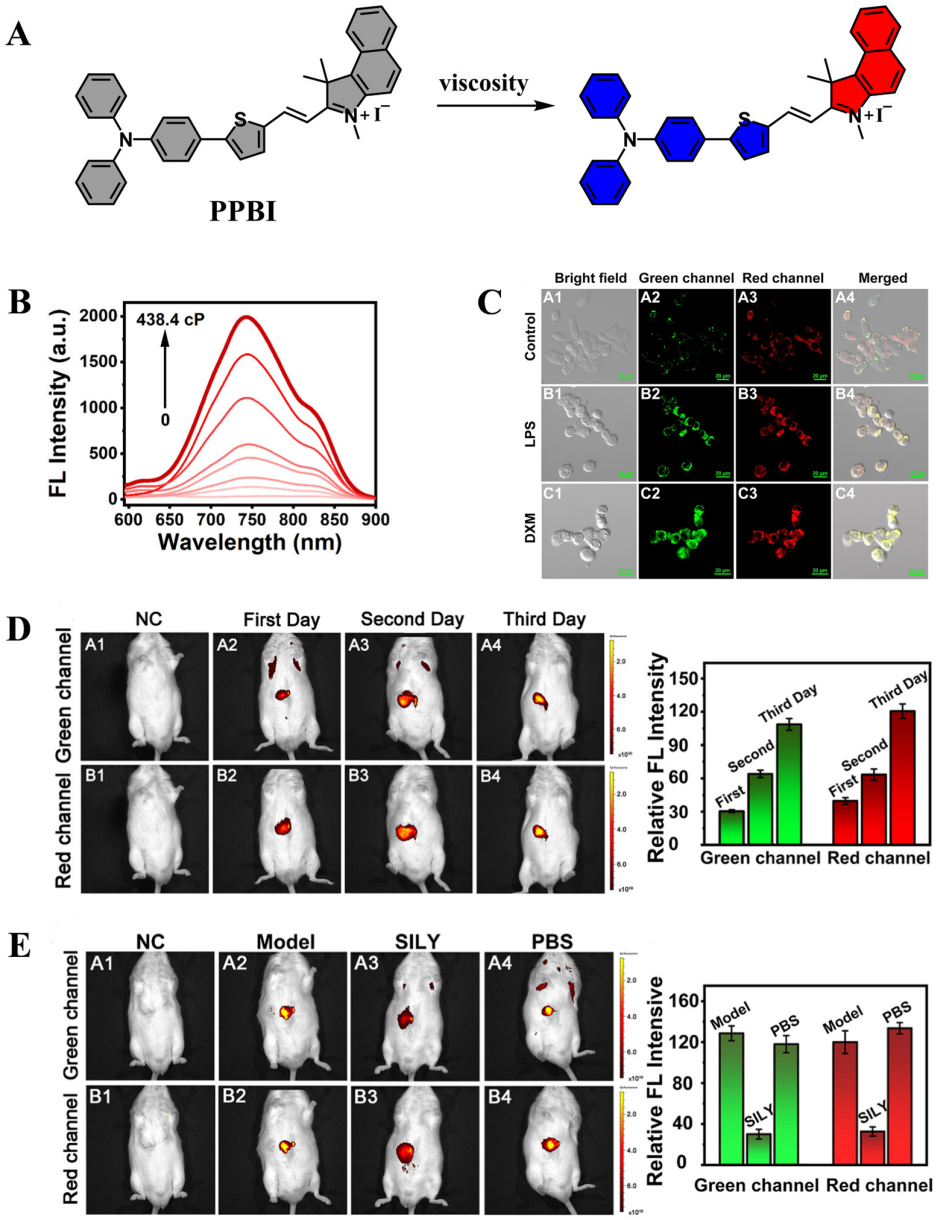


Figure 3. (**A**) Polarity/viscosity response mechanism of the fluorescent probe PPBI. (**B**) Fluorescent spectra of probe PPBI (10 μM) in PBS-glycerol mixture solution of different viscosities (0.89–438.4 cP). (**C**) Confocal laser scanning images of HepG2 cells, Control: the cells were pretreated with PPBI (10 μM) only LPS: the cells were pretreated with 20 μM LPS for 30 min and then incubated with PPBI (10 μM) for another 60 min, DXM: the cells were pretreated with 20 μM DXM for 30 min and then incubated with PPBI (10 μM) for another 60 min. (**D**) Time-dependent in vivo fluorescent imaging and relative fluorescent intensity of mice after intrahepatic injection of PPBI (10 μM) and continuous treatment with alcohol. (**E**) In vivo fluorescent imaging and relative fluorescence intensity of PPBI (10 μM) in normal contrast mice, model mice, SILY- and PBS-treated mice, respectively. Scale bar: 50 μm. Derived from Ref. [33] with authorization from Copyright 2023, Elsevier.

Yang et al. designed a dual-ratiometric fluorescent probe (WTH) based on phenothiazine-coumarin and hydroxycoumarin derivatives, capable of simultaneously detecting HClO and H_2O_2 (Figure 2G). The probe exhibited high sensitivity, selectivity, and stability across a broad pH range. Using confocal microscopy, researchers successfully imaged HClO and H_2O_2 levels in living cells and zebrafish, confirming the probe's ability to monitor oxidative stress changes during ALI (Figure 4). This study provides a valuable tool for understanding ALI-related inflammation and oxidative stress mechanisms [34].

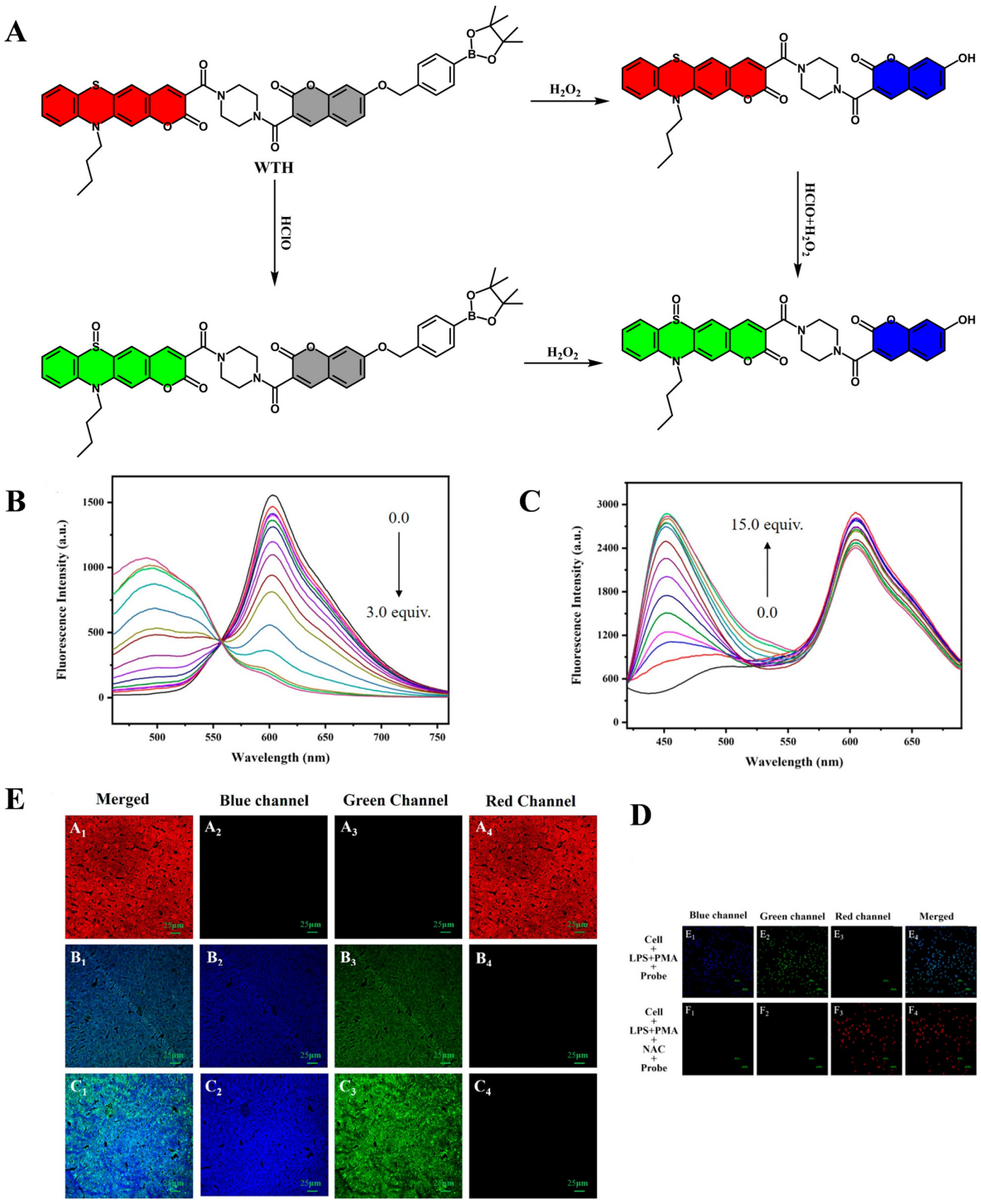


Figure 4. (**A**) H_2O_2/HClO response mechanism of the fluorescent probe WTH. (**B**,**C**) Fluorescence spectral changes of WTH in response to varying amounts of HClO and H_2O_2. (**D**) Imaging of endogenous HClO and H_2O_2 in HepG2 cells. (**E1**–**E4**) Cells cultivated with LPS (1 μg/mL) and PMA (1 μg/mL) for 1 h and then cultivated with probe 1 for 20 min. (**F1**–**F4**) Cells cultivated with LPS (1 μg/mL) and PMA (1 μg/mL) for 1 h, NAC (1.0 mM) for 1 h, and probe 1 for 20 min. (**E**) Imaging of alcoholic liver injury in mice. Fluorescence imaging of liver tissue of control mice (**A1**–**A4**), liver tissue of group 1 mice (**B1**–**B4**), and liver tissue sections of group 2 mice (**C1**–**C4**). Blue channel, Ex = 405 nm, Em = 450 ± 25 nm; green channel, Ex = 488 nm, Em = 525 ± 25 nm; red channel, Ex = 488 nm, Em = 595 ± 25 nm. Derived from Ref. [34] with authorization from Copyright 2022, American Chemical Society.

Zhang et al. synthesized a near-infrared fluorescent probe (BDP-NIR-ONOO) featuring a BODIPY dye core and an aryl boronic acid detection moiety, designed for real-time visualization of ALI (Figure 2H). The probe demonstrated high specificity, rapid response, and a high signal-to-noise ratio in vitro. BDP-NIR-ONOO successfully detected $ONOO^-$ fluctuations in ALD mouse models, providing a valuable tool for ALI diagnosis and inflammation research [35].

Zhou et al. designed and synthesized the Cy-ND probe, which exhibits significant sensitivity to viscosity changes in biological environments (Figure 2I). This probe also offers low cytotoxicity and minimal background interference, making it effective for identifying variations in biological viscosity. The Cy-ND probe successfully detected viscosity changes in models of acute alcohol-induced liver injury and liver ischemia-reperfusion injury, providing a valuable tool for further research on liver injury in animal models [36].

Hai et al. designed and synthesized the WZ-HOCl fluorescent probe, which exhibits rapid response and excellent selectivity for HOCl detection (Figure 2J). Furthermore, WZ-HOCl can distinguish between HepG2 and L02 cells, providing a novel approach for liver cancer detection. The probe has also successfully detected HOCl in models of alcoholic hepatitis, non-alcoholic fatty liver disease, and various inflammation-related diseases. WZ-HOCl holds significant potential for early clinical diagnosis and disease screening [37].

3. Chemical Liver Injury

3.1. Establishment of Chemical Liver Injury Models

CLI refers to liver function impairment caused by exposure to exogenous chemicals, including drugs, toxic compounds, and industrial chemicals. Its pathological mechanisms are complex and are closely linked to the direct toxic effects of active metabolites generated during hepatic metabolism as well as the subsequent inflammatory response. Depending on exposure mode and duration, CLI can be classified into acute CLI and chronic CLI. Acute CLI typically results from short-term exposure to high doses of toxic chemicals, such as CCl_4 or industrial solvents, leading to hepatocellular necrosis, increased oxidative stress, and an amplified inflammatory response. In severe cases, acute liver failure may occur. Chronic CLI is mainly induced by long-term exposure to low-dose toxicants, such as prolonged drug abuse or environmental toxin exposure, which gradually leads to hepatic fibrosis, fatty degeneration, and even cirrhosis.

CCl_4 is a widely studied hepatotoxin in liver toxicology due to its strong hepatotoxic effects, which can induce hepatic degeneration, fibrosis, carcinogenesis, and necrosis. Therefore, it is commonly used to establish acute CLI models. The hepatotoxicity of CCl_4 is dose- and time-dependent [38]. Upon metabolic activation by cytochrome P450 enzymes, CCl_4 generates trichloromethyl radicals and trichloromethyl peroxide radicals. These highly reactive metabolites interact with sulfhydryl-containing proteins, altering cell membrane fluidity and permeability, thereby inducing lipid peroxidation, damaging organelles (especially mitochondria), and ultimately triggering hepatocyte death [39,40].

Additionally, CCl_4-mediated liver damage is further exacerbated by the production of ROS and RNS, such as NO. At low concentrations, NO improves hepatic microcirculation, whereas at high concentrations, it accelerates liver damage [41]. Moreover, CCl_4 activates hepatic macrophages and Kupffer cells, stimulating the secretion of pro-inflammatory cytokines such as TNF-α, IL-1, and IL-6, further recruiting neutrophils, amplifying oxidative stress, and aggravating hepatocellular damage [42,43].

CCl_4-induced liver injury is also closely associated with apoptosis pathways. TNF-α can activate apoptotic proteins via the p55TNF receptor, leading to programmed cell death. Moreover, excess ROS disrupts mitochondrial function, promoting cytochrome C release and activating the mitochondrial apoptosis pathway [44,45].

To establish a CCl_4-induced liver injury model, rats or mice are commonly used. Intraperitoneal injection or oral gavage is the preferred administration route (Figure 5). Typically, CCl_4 is diluted in vegetable oil at a ratio of 1:1 to 1:3, and adult rats receive intraperitoneal or oral doses of 0.8–1.6 mL/kg body weight [46]. Since mice are more sensitive to CCl_4 toxicity, a lower concentration (0.1–1% CCl_4 in vegetable oil) is used, with doses of 10–20 mL/kg body weight administered via oral gavage or intraperitoneal injection [47,48]. After 12–24 h, hepatic function, lipid peroxidation markers, and histopathological changes are evaluated.

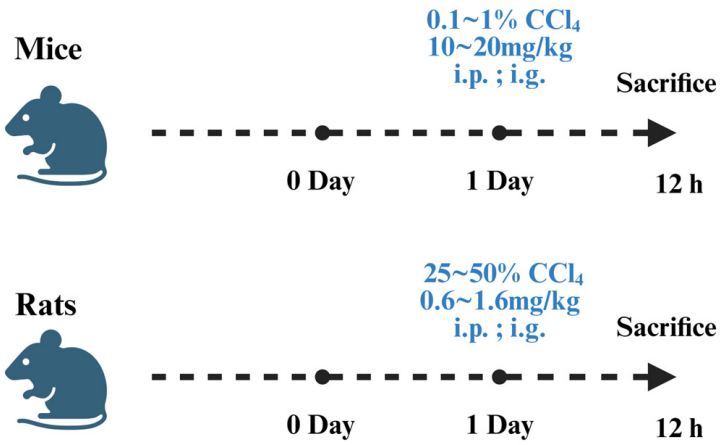


Figure 5. Schematic representation of CCl_4-induced liver injury in animal models.

The CCl_4-induced liver injury model accurately reflects hepatic functional, metabolic, and morphological alterations. This model is widely used due to its low technical requirements, reproducibility, and easy implementation. However, its effects are influenced by factors such as sex, dosage, and exposure duration, making precise experimental control essential. Meanwhile a large number of fluorescent probes for the detection of CLI already exist (Table 2).

Table 2. Characterization of fluorescent probes in the CLI model.

Compounds	Trigger	λex (nm)	λem (nm)	Ref.
YG-H_2S	H_2S	375	520	[49]
NRh-NNBA	GSTs	850	832	[50]
PX-1	$ONOO^-$	405	553	[51]
Lyso-ONOO	$ONOO^-$	450	555	[52]
NIR-II Cy3-988	HClO	980	1048	[53]
HZY	SO_3^{2-}	380	470	[54]
HM-ASPH-PF	MPO	400	586	[55]
Golgi-PER	$ONOO^-$	395	520/415	[56]
PC-Py	HOCl	420	570	[57]

3.2. Application of Fluorescent Probes in Chemical Liver Injury

Yang et al. developed YG-H_2S, a novel H_2S-responsive fluorescent probe, for imaging H_2S dynamics in CLI models (Figure 6A). Compared to traditional probes, YG-H_2S exhibits faster response kinetics, higher selectivity, and stability across a broad pH range, minimizing background noise from complex hepatic environments. Designed based on a deep understanding of H_2S metabolism dynamics, YG-H_2S enables precise localization

of pathological sites while also elucidating the role of H_2S in free radical regulation. In CCl_4-induced acute liver injury models, YG-H_2S successfully visualized H_2S fluctuations, correlating its levels with injury severity (Figure 7). Moreover, its low cytotoxicity makes it well-suited for deep tissue imaging in live organisms [49].

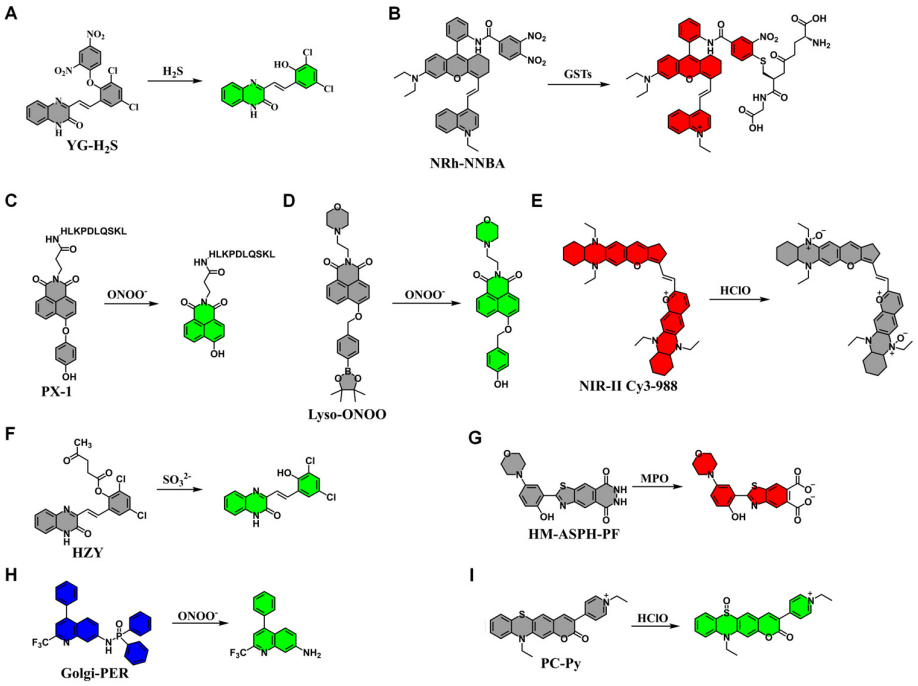


Figure 6. (**A**–**I**) Structure and detection mechanism of fluorescent probe in CLI models.

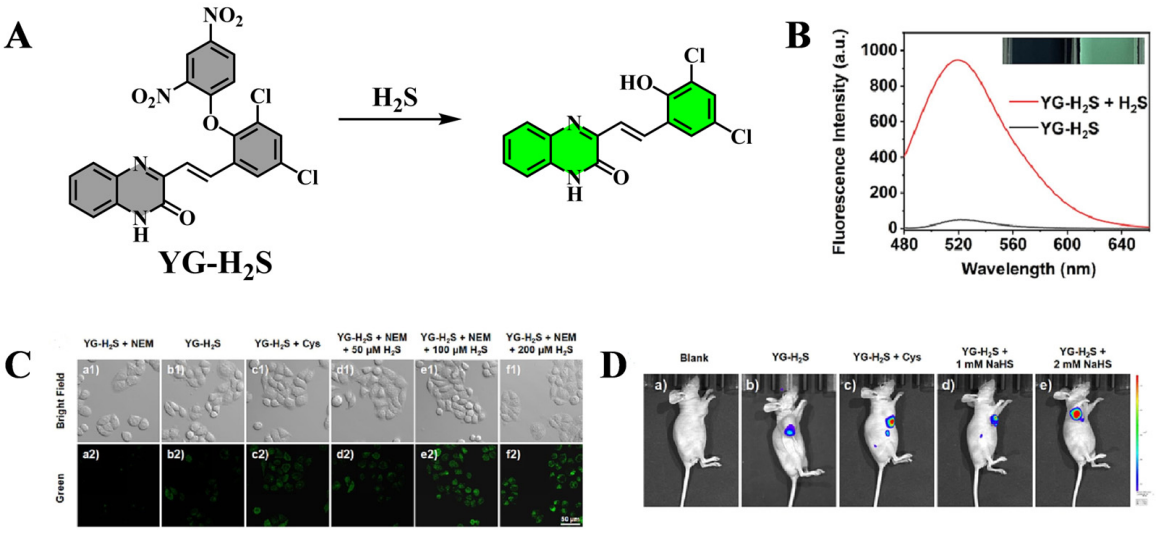


Figure 7. (**A**) H_2S response mechanism of the fluorescent probe YG-H_2S. (**B**) Fluorescence spectra of YG-H_2S (10 μM) in the absence and presence of H_2S in PBS buffer (10 mM, 1% DMSO, pH 7.4). Insert: the UV light of YG-H_2S (10 μM) without and with H_2S. (**C**) Confocal images of living HeLa cells with YG-H_2S (20 μM) under different treating conditions. (**D**) The fluorescence imaging of YG-H_2S (100 μM) in the 4T1-xenograft mice under various conditions. (**a**) Blank mice (**b**) Intravenous injection with YG-H_2S (100 μM); (**c**) Pre-treatment with Cys (2 mM) and then intravenous injection with YG-H_2S (100 μM); (**d**,**e**) Pre-treatment with NaHS and then intravenous injection with YG-H_2S (100 μM). Derived from Ref. [49] with authorization from Copyright 2023, Elsevier.

Wang et al. developed NRh-NNBA, a rhodamine-based upconversion luminescence probe, for the detection of GSTs in CLI models (Figure 6B). In CCl_4-induced CLI, NRh-

NNBA exhibited rapid and specific responsiveness to GSTs. The probe successfully quantified endogenous GSTs in human liver L02 cells, liver tissue sections, and mouse serum samples, offering a high signal-to-noise ratio. Furthermore, its upconversion luminescence properties effectively reduce autofluorescence interference in biological samples. These findings suggest that NRh-NNBA is a promising sensor for GST-based CLI diagnosis and monitoring [50].

Tang et al. developed PX-1, a non-peptide-based two-photon fluorescent probe, designed for $ONOO^-$ detection in CLI models (Figure 6C). PX-1 features high sensitivity, rapid response, and precise targeting capabilities. In vitro, PX-1 demonstrated excellent specificity and sensitivity for $ONOO^-$. Furthermore, in vivo imaging of CCl_4-induced CLI models revealed significantly upregulated $ONOO^-$ levels in injured livers. This work provides a new strategy for elucidating the physiological role of $ONOO^-$ in acute liver injury [51].

Yang et al. developed Lyso-ONOO, a fluorescent probe for $ONOO^-$ tracking in CLI mouse models (Figure 6D). Lyso-ONOO exhibited high selectivity, sensitivity, and resistance to interference, making it effective for monitoring $ONOO^-$ fluctuations in LX-2 cells. Moreover, its strong lysosomal targeting ability allowed for accurate visualization of $ONOO^-$ dynamics during CLI progression and therapeutic interventions. Both in vivo fluorescence imaging and deep-tissue imaging confirmed Lyso-ONOO's capability to correlate $ONOO^-$ levels with liver injury severity and therapeutic efficacy, providing a promising tool for assessing different treatment strategies [52].

Yuan et al. developed NIR-II Cy3-988, a NIR-II fluorescent probe, capable of selective HClO detection (Figure 6E). Notably, NIR-II Cy3-988 is reversible, allowing dynamic monitoring of HClO/RSS-mediated redox fluctuations. The probe was successfully applied to detect oxidative microenvironment alterations in acute inflammation and CLI repair models, as well as evaluate drug efficacy during acute inflammation. These findings suggest that NIR-II Cy3-988 is a valuable tool for precise real-time imaging of redox dynamics [53].

Hu et al. designed HZY, a fluorescent probe for SO_3^{2-} detection, which exhibits high specificity, rapid response, and a large Stokes shift (Figure 6F). HZY successfully visualized SO_3^{2-} levels in vitro and in vivo, tracking dynamic changes during CLI progression and treatment in CCl_4-induced models (Figure 8). These findings highlight HZY's potential for in situ SO_3^{2-} detection, making it a promising tool for CLI preclinical diagnosis and clinical applications [54].

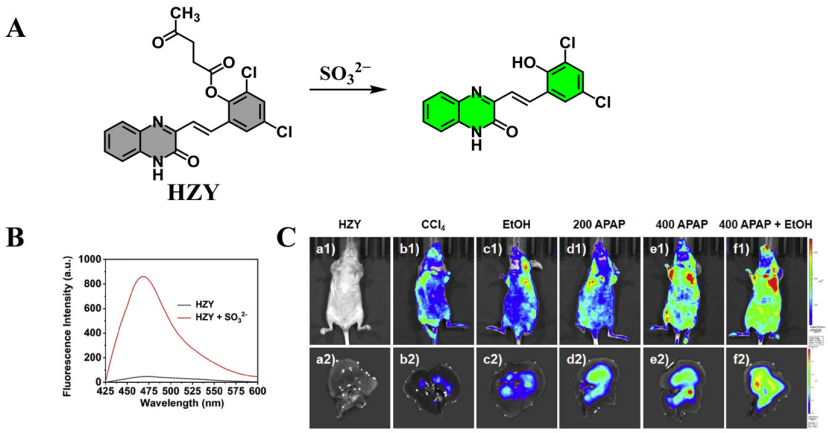


Figure 8. (**A**) SO_3^{2-} response mechanism of the fluorescent probe HZY. (**B**) The fluorescence of HZY with or without SO_3^{2-} in PBS buffer. (**C**) Intravenous injection of HZY in mice with normal and ALI. Liver tissues were dissected to perform in vivo imaging. Derived from Ref. [54] with authorization from Copyright 2023, Elsevier.

Duan et al. synthesized HM-ASPH-PF, a luminol-based fluorescent probe for MPO detection (Figure 6G). The probe, featuring benzothiazole and cyclic phthalic acid hydrazide moieties, exhibits high selectivity, sensitivity, stability, and excellent water solubility. HM-ASPH-PF successfully imaged MPO activity in ALI and acute liver failure mouse models, providing a novel approach for developing orange-emitting luminol derivatives and evaluating neutrophil-associated liver diseases [55].

Liu et al. designed Golgi-PER, a ratiometric fluorescent probe for $ONOO^-$ detection, which exhibited high sensitivity, a low detection limit, and excellent selectivity (Figure 6H). Golgi-PER efficiently tracked $ONOO^-$ levels in CCl_4-induced CLI models, correlating its fluctuations with disease progression and treatment response. These results suggest that Golgi-PER is a valuable tool for investigating liver disease pathogenesis and therapeutic strategies [56].

Wang et al. synthesized PC-Py, a highly selective HOCl-responsive fluorescent probe (Figure 6I). PC-Py exhibits fast response, high sensitivity, and excellent membrane permeability, allowing for accurate HOCl detection during CLI progression. Furthermore, PC-Py successfully differentiated liver fibrosis, acute liver injury, and cirrhosis by monitoring HOCl fluctuations. These findings highlight PC-Py's potential for HOCl-based liver disease diagnosis [57].

4. Drug-Induced Liver Injury

4.1. Establishment of Drug-Induced Liver Injury Models

DILI refers to hepatic damage caused by the toxic effects of drugs or their metabolites, as well as immune-mediated hypersensitivity reactions during pharmacological treatment [58]. The mechanisms underlying DILI are complex and can be broadly classified into two categories [59]. Idiosyncratic DILI arises from specific pharmacological effects of certain drugs, making its occurrence unpredictable by conventional screening methods. Although rare, idiosyncratic DILI is often severe and can lead to acute liver failure. In contrast, intrinsic DILI is associated with dose-dependent toxicity, typically resulting from drug overdose or the overloading of hepatic detoxification pathways, making its onset more predictable [60,61].

APAP is a widely used over-the-counter antipyretic and analgesic, and its hepatotoxicity is among the most common causes of DILI. Due to its well-characterized mechanisms, APAP-induced liver injury serves as a reliable experimental model for studying the pathogenesis, prevention, and treatment of DILI [62,63]. The hepatotoxicity of APAP is primarily mediated by its highly reactive metabolite, NAPQI, which targets mitochondrial proteins and forms covalent adducts with key hepatocellular components, including housekeeping proteins, glutathione peroxidase, and the α-subunit of ATP synthase [64,65]. The disruption of mitochondrial function by NAPQI leads to electron leakage in the electron transport chain, promoting the generation of superoxide radicals [66]. These radicals undergo further conversion into H_2O_2 and molecular oxygen through the action of manganese superoxide dismutase or react with endogenous NO to form $ONOO^-$ [67]. The accumulation of oxidative stress markers such as $ONOO^-$ contributes to mitochondrial damage, ultimately exacerbating hepatocyte injury.

The detoxification of H_2O_2 in hepatocytes primarily relies on GSH and enzymatic clearance by antioxidant systems, including glutathione peroxidase, catalase, and peroxiredoxin. However, during APAP-induced hepatotoxicity, mitochondrial cysteine reacts with GSH, further depleting antioxidant reserves and amplifying hepatic damage. The excessive accumulation of ROS and peroxynitrite leads to the depletion of GSH, the formation of nitrotyrosine-protein adducts, and mitochondrial DNA damage, collectively resulting in extensive liver cell necrosis and apoptosis. These molecular events make

APAP-induced hepatotoxicity a well-established model for investigating oxidative stress, lipid peroxidation, and mitochondrial dysfunction in DILI.

The APAP-induced acute liver injury model is widely used due to its ability to closely replicate human DILI pathogenesis. The most common experimental approach involves oral gavage or intraperitoneal injection of APAP in mice to induce hepatotoxicity (Figure 9). Sun et al. developed a DILI mouse model by fasting male C57BL/6J mice for 16 h, followed by intraperitoneal injection of 400 mg/kg APAP. After 12 h, liver and blood samples were collected for biochemical analysis [68]. Liang et al. established a similar model using Kunming mice, where animals were fasted for 24 h before receiving a 250 mg/kg intraperitoneal dose of APAP, with sampling conducted four hours post-injection [69]. Jiang et al. induced DILI by administering 300 mg/kg APAP intraperitoneally to male C57BL/6 mice following a seven-day adaptive feeding period, with liver samples collected 12 h later [70].

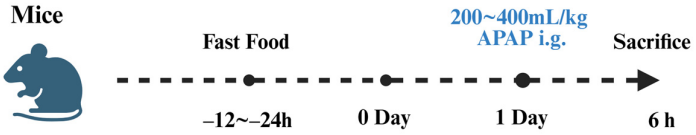


Figure 9. Schematic diagram of animal models for DILI.

The APAP-induced liver injury model offers high reproducibility and precise control over experimental variables, allowing researchers to closely examine oxidative stress, lipid peroxidation, DNA damage, and protein dysfunction. With a short modeling time and strong clinical relevance, this model serves as an optimal platform for studying the protective effects of natural compounds and pharmacological interventions against DILI. Meanwhile a large number of fluorescent probes for the detection of DILI already exist (Table 3).

Table 3. Characterization of fluorescent probes in the DILI model.

Compounds	Trigger	λex (nm)	λem (nm)	Ref.
LW-OTf	$O_2^{\bullet-}$ $ONOO^-$	670 360	715 461	[71]
ATP-LW	$ONOO^-$ ATP	450, 488 520	562, 568 587	[72]
VIS-HNO	HNO Viscosity	427 405	637 475	[73]
NOP	$ONOO^-$	580	656	[74]
IR-990	H_2O_2	808	990	[75]
RPC-1	H_2S HClO	360 545	445 580	[76]
RNH-X	HClO	442	500/710	[77]
Fluo-HNO	HNO	480	520	[78]
Mito-HNO	HNO	695	725	[78]
DOP-CO	CO	630	785/720	[79]
P-GST	GSH	420	550	[80]

4.2. Application of Fluorescent Probes in Drug-Induced Liver Injury

James et al. developed a near-infrared fluorescent probe LW-OTf, which consists of a triflate functional group and a cyanine dye, designed to detect $O_2^{\bullet-}$ and $ONOO^-$ during

DILI (Figure 10A). The probe enables in situ imaging of RNS and ROS in HL-7702 cells with APAP-induced hepatotoxicity. In vivo experiments demonstrated an increase in $O_2^{\bullet-}$ and $ONOO^-$ levels in DILI mouse livers, which was confirmed by SC (H&E) staining, validating the formation of DILI [71].

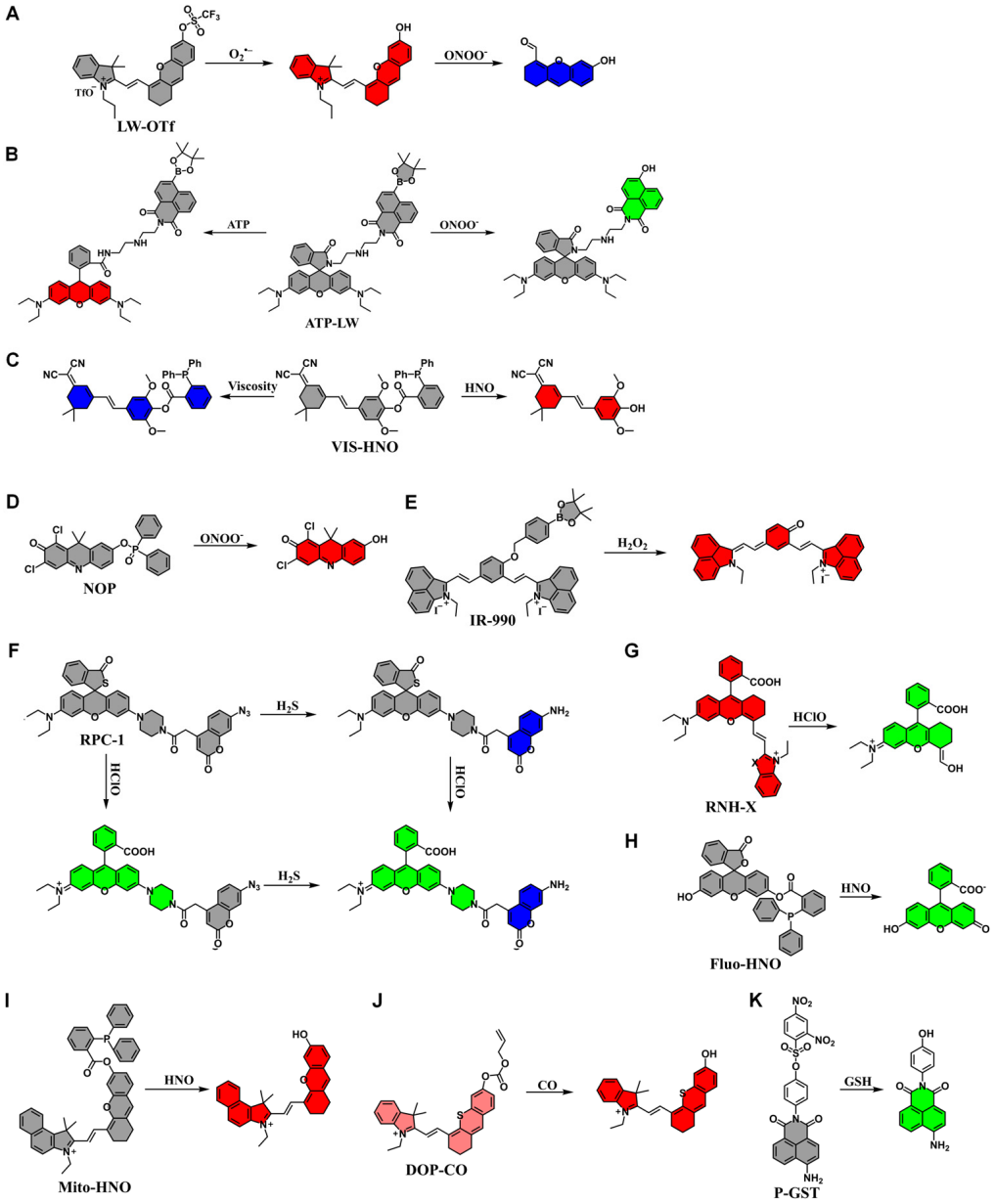


Figure 10. (**A**–**K**) Structure and detection mechanism of fluorescent probe in DILI models.

Sessler et al. reported ATP-LW, a hybrid fluorescent probe incorporating rhodamine lactam and 1,8-naphthalimide, capable of detecting $ONOO^-$ and ATP simultaneously (Figure 10B). When $ONOO^-$ was present, fluorescence emission was observed at 500–575 nm, whereas in the presence of ATP, rhodamine lactam ring opening resulted in fluorescence at 575–650 nm. Imaging of HL-7702 cells treated with oligomycin A revealed a decrease in red fluorescence and an increase in green fluorescence, indicating ATP depletion and $ONOO^-$ accumulation. Similar results were obtained when cells were treated with SIN-1. Further imaging of APAP-induced hepatotoxicity confirmed $ONOO^-$ elevation and ATP depletion, making ATP-LW a promising probe for simultaneous monitoring of oxidative stress and energy metabolism during DILI [72].

Ye et al. synthesized VIS-HNO, a dual-response fluorescent probe for HNO and viscosity, with high sensitivity, selectivity, and biocompatibility (Figure 10C). VIS-HNO enables independent evaluation of HNO and viscosity without cross-interference and was successfully applied to bioimaging in living cells and zebrafish, revealing the role of HNO in DILI. By assessing HNO and viscosity levels, VIS-HNO provides a valuable tool for DILI diagnosis, ferroptosis research, and therapeutic intervention studies [73].

Li et al. designed NOP, a fluorescent probe with high stability, broad pH adaptability, and superior specificity and sensitivity for $ONOO^-$ detection (Figure 10D). In the APAP-induced liver injury model, NOP successfully monitored $ONOO^-$ level fluctuations, with fluorescence signals correlating with histopathological staining and serum biomarker analysis (Figure 11). These results demonstrate that NOP is an effective tool for early DILI diagnosis, mechanistic studies, and therapeutic screening [74].

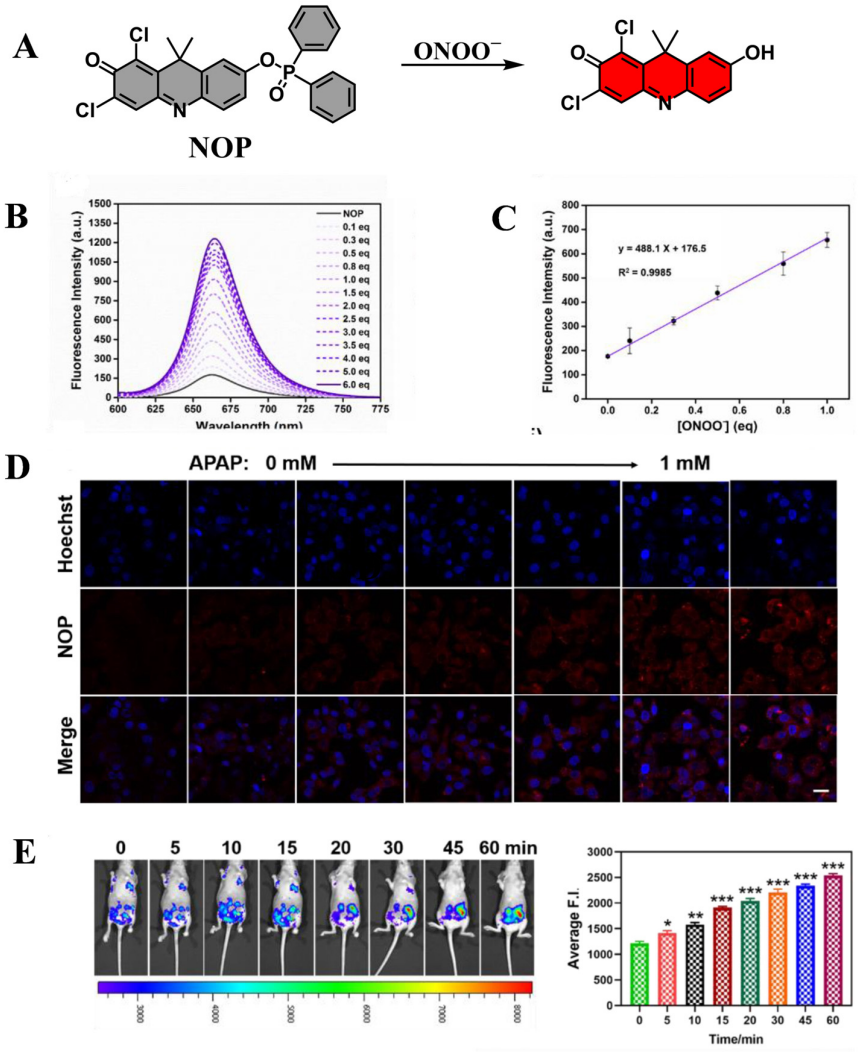


Figure 11. (**A**) $ONOO^-$ response mechanism of the fluorescent probe NOP. (**B**) Fluorescence spectra of 10 μM NOP and 0–60 μM $ONOO^-$ for 5 min. (**C**) The linear relationship between NOP (10 μM) and $ONOO^-$ (from 0 to 10 μM). (**D**) HepG2 cells were coincubated with APAP (0, 0.1, 0.2, 0.4, 0.6, 0.8, 1.0 mM) for 12 h, then the cells were washed with PBS three times. After added the NOP (10 μM) for 30 min. Finally, commercial Hoechst 33,342 dye was added and stained for 15min. Scale bar: 25 μM. (**E**) The nude mice were intraperitoneally injected with 100 μM NOP (200 μL in normal saline (NS)), and then intraperitoneally injected with 500 μM $ONOO^-$ at the same location. After fluorescence images and fluorescence intensity of mice were collected at different time points: 0, 5, 10, 15, 20, 30, 45, 60 min. ∗ p-value < 0.05, ∗∗ p-value < 0.01, ∗∗∗ p-value < 0.001. Derived from Ref. [74] with authorization from Copyright 2023, Elsevier.

Xiong et al. synthesized IR-990, a NIR-II fluorescent probe designed for H_2O_2 detection (Figure 10E). The receptor-π-receptor framework of IR-990 ensures high sensitivity, large Stokes shift, and low detection limits. IR-990 successfully tracked endogenous H_2O_2 variations in HepG2 cells and DILI mouse models, providing real-time imaging capabilities. As a powerful diagnostic tool, IR-990 enables H_2O_2 visualization in vivo, offering great potential for elucidating DILI pathogenesis [75].

Tang et al. developed RPC-1, a two-photon fluorescent probe for simultaneous differentiation and imaging of H_2S and HClO (Figure 10F). The probe was used to evaluate DILI induced by the antidepressants duloxetine and fluoxetine, revealing significant HClO upregulation and severe liver damage after co-administration. The correlated changes in HClO and H_2S levels confirmed the protective role of endogenous H_2S. Histological and serological analyses further validated HClO as a reliable DILI marker and H_2S as a potential therapeutic target, demonstrating RPC-1's utility in DILI prediction and antidote research [76].

Liu et al. designed RNH-X, a mitochondria-targeted ratiometric fluorescent probe for HClO detection in APAP-induced liver and kidney injury (Figure 10G). RNH-O, the most reactive derivative, exhibited high sensitivity, rapid response, and excellent selectivity. The probe successfully tracked HClO fluctuations in living cells, detected APAP-induced HClO upregulation, and enabled fluorescence imaging of inflammatory tissues in DILI mouse models, making it a valuable tool for assessing liver and kidney damage (Figure 12) [77].

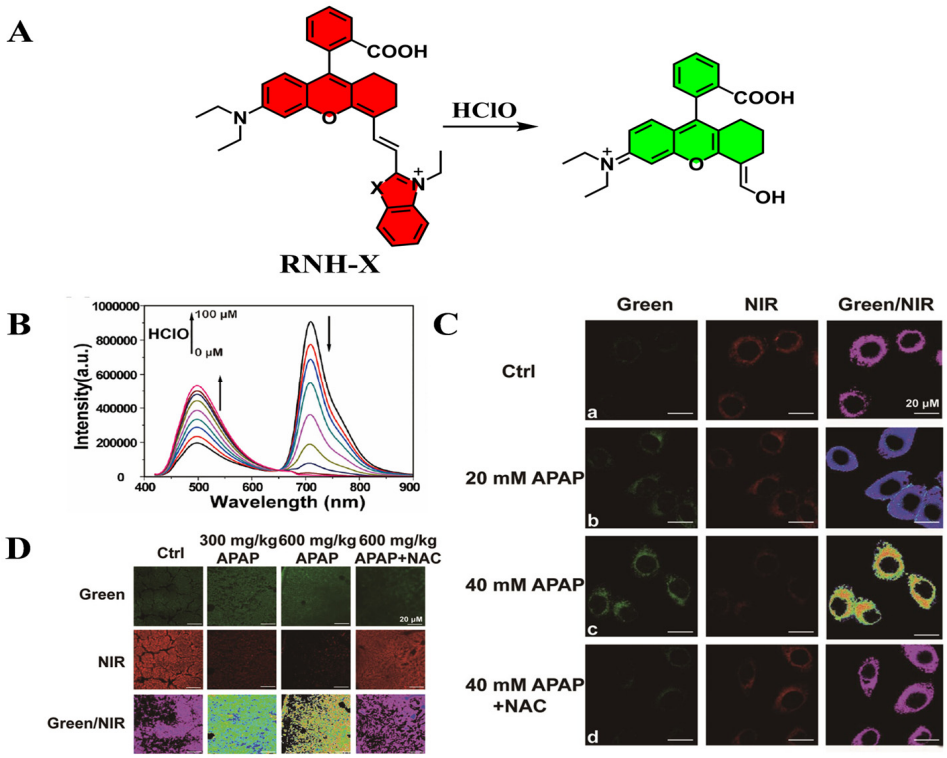


Figure 12. (**A**) HClO response mechanism of the fluorescent probe RNH-X. (**B**) Fluorescence value of the probe NRH-O (10 μM) at diverse concentrations of HClO (0–10 equiv.). (**C**) Confocal fluorescence imaging of human normal liver L02 cells at different fluorescence channels; scale bar is 20.0 μM. Cells were incubated with different contents of APAP (20, 40 mM), NAC (40 mM), and incubated with NRH-O (10 μM) for half an hour before imaging. (**D**) Fluorescence imaging of liver tissue slices from mice after intraperitoneal injection of NRH-O 10 μL (10 mM) after 1 h. Derived from Ref. [77] with authorization from Copyright 2022, American Chemical Society.

The production of RNS, such as HNO, is known to be an early signal of DILI (Figure 10H). Tang and colleagues developed Fluo-HNO as a specific fluorescent probe for

in situ imaging of HNO in the Golgi apparatus. This work demonstrated for the first time that catalase plays a role in the production of intracellular HNO. The probe enables the detection of HNO concentration changes in the liver, providing a powerful tool for DILI diagnosis [78].

Tang's team also developed Mito-HNO, a specific fluorescent probe for in situ imaging of HNO in mitochondria (Figure 10I). Like Fluo-HNO, Mito-HNO enables multicolor imaging and provides detailed insights into HNO levels in the mitochondria of liver cells. Their study revealed that the concentration of HNO in the liver of mice induced by the anticancer drug bleomycin was significantly increased. These findings underscore the potential of HNO as a diagnostic marker for DILI, offering valuable information for liver injury assessment [78].

Chen et al. developed DOP-CO, a photoacoustic/fluorescence dual-mode imaging probe for CO detection, utilizing thione-semicyanine as the core structure (Figure 10J). The probe exhibited excellent biocompatibility and enabled quantitative CO detection in HepG2 cells. In vivo studies demonstrated CO fluctuations in liver injury and repair, providing insights into CO-mediated hepatoprotective mechanisms and making DOP-CO a promising tool for investigating CO-related physiological and pathological processes [79].

Feng et al. developed P-GST, a two-photon fluorescent probe for GST detection, utilizing a naphthalimide skeleton with a 2,4-dinitrobenzenesulfonyl recognition unit (Figure 10K). In the presence of GST and GSH, the recognition unit is cleaved, releasing fluorescence. P-GST was successfully applied to two-photon imaging of GST in DILI models, confirming its diagnostic potential for monitoring GST activity in complex biological systems [80].

5. Immune Liver Injury

5.1. Establishment of the LPS-Induced Liver Injury Models

ILI refers to hepatic damage triggered by abnormal immune responses, which involve autoimmune activation or responses to exogenous factors. The underlying pathological mechanisms primarily include immune cell-mediated attacks on hepatocytes or bile duct epithelial cells, excessive inflammatory cytokine release, and immune regulatory dysfunction [81,82]. Based on etiological factors, ILI can be classified into autoimmune liver injury and immune-mediated liver injury induced by drugs or infections. Autoimmune liver injury includes autoimmune hepatitis, primary biliary cholangitis, and primary sclerosing cholangitis, with pathogenesis closely linked to genetic predisposition, environmental factors (such as infections), and immune dysregulation. The main mechanism involves autoantigen exposure or abnormal antigen presentation, leading to T cell-mediated immune attacks [83,84]. Immune liver injury induced by drugs or infections is caused by immune checkpoint inhibitors or pathogenic infections (e.g., viral infections), which provoke an immune overreaction against liver tissues. This type of ILI is characterized by high individual variability, with drugs or infections acting as initiating triggers [85].

LPS is widely used in experimental models to mimic ILI due to its ability to elicit strong inflammatory responses via the TLR4 signaling pathway. LPS-induced liver injury effectively models exogenous infection-related immune activation and serves as a key tool for studying immune-mediated hepatic inflammation, oxidative stress, and apoptosis. Following entry into the bloodstream, LPS binds to lipopolysaccharide-binding protein and is transported via CD14 to the TLR4/myeloid differentiation protein-2 complex, leading to TLR4 dimerization and activation [86–88]. The activated TLR4 pathway stimulates NF-κB signaling through myeloid differentiation factor 88, thereby inducing inflammatory cytokine transcription and promoting acute inflammatory responses [89,90]. Upon NF-κB/p65 complex nuclear translocation, the expression of TNF-α, IL-1β, and IL-6 is

upregulated, further exacerbating hepatic damage [91]. The severity of TLR4-mediated liver injury is dependent on NF-κB activation, which not only amplifies inflammatory responses but also enhances oxidative stress and apoptosis, leading to progressive liver pathology.

Studies have demonstrated that LPS activates Kupffer cells, triggering the release of ROS, proinflammatory cytokines, and chemokines, thereby promoting neutrophil infiltration and further aggravating hepatic damage [92]. The inflammatory cascade induced by LPS also activates anti-inflammatory cytokines such as IL-1RA, IL-4, IL-10, and IL-13 as part of a feedback regulation mechanism [93]. LPS-induced hepatic inflammation is characterized by increased TLR4 expression, excessive immune activation, and potential cellular damage, septic shock, or multi-organ failure. By administering intraperitoneal injections of LPS, researchers can simulate exogenous infections and construct experimental models of inflammatory liver injury. LPS-stimulated Kupffer cells generate ROS, proinflammatory mediators, and chemokines, which drive neutrophil infiltration, thereby reproducing key pathological features of immune-mediated hepatic injury.

Experimental models of LPS-induced liver injury have been successfully established in different mouse strains through intraperitoneal injection of LPS, leading to acute hepatic inflammation (Figure 13) [94]. Wang et al. developed an acute liver injury model using ICR mice, where 15 mg/kg of LPS was administered intraperitoneally, and hepatic damage was confirmed 12 h post-injection through histopathological and biochemical analyses [95]. Jia et al. established a similar model in Kunming mice, administering 5 mg/kg of LPS daily for three consecutive days, with one injection per day to induce progressive liver inflammation [96]. Miao et al. further optimized the model by injecting 3 mg/kg of LPS intraperitoneally in Kunming mice, and analyzing liver injury six hours post-injection [97].

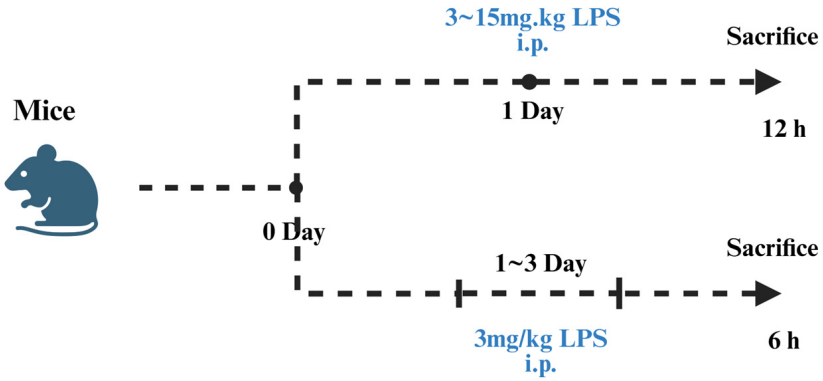


Figure 13. Schematic representation of LPS-induced liver injury in animal models.

This LPS-induced liver injury model offers high reproducibility and scalability, allowing researchers to replicate inflammatory hepatic damage across different animal groups. The model is simple to establish, with a short induction period and adjustable LPS dosages, making it a valuable platform for investigating immune-mediated hepatic inflammation, oxidative stress, and drug intervention strategies. The flexibility of this model also allows for combining LPS administration with additional treatments to simulate various pathological conditions in liver disease research. Meanwhile a large number of fluorescent probes for the detection of LPS-induced liver injury already exist (Table 4).

Table 4. Characterization of fluorescent probes in LPS-Induced Liver Injury.

Compounds	Trigger	λex (nm)	λem (nm)	Ref.
NIR-II-H_2S_2	H_2S_2	730, 808	840, 1000	[98]
AP-Sn	H_2Sn	660	715	[99]
Mito-ND	Viscosity	560	676	[100]
MNIP-Cu	NO	350	492	[101]
DHBP	Viscosity Polarity	450 480	630 660	[102]
KSQT	HOCl	405	475/589	[103]
SPN	$ONOO^-$	680	732	[104]
RDB-ClO	ClO^-	380	582/455	[105]
BDP-R-ClO	HOCl	560	661	[106]

5.2. Application of Fluorescent Probes in LPS-Induced Liver Injury

H_2S_2 plays a crucial role in redox biology and cellular signaling [107]. The ability to quantitatively visualize H_2S_2 in deep tissues is essential for understanding pathophysiological mechanisms related to immune liver injury. Chen et al. successfully developed NIR-II-H_2S_2, a dual-ratiometric NIR-II fluorescent probe designed for selective H_2S_2 detection, featuring a 1,3-dichloro recognition moiety and an NIR-II fluorophore scaffold (Figure 14A). The probe demonstrated high specificity, excellent sensitivity, and enhanced water solubility, as well as deep tissue penetration, making it suitable for real-time imaging of H_2S_2 levels in LPS-induced liver injury models. These findings highlight the potential of NIR-II-H_2S_2 as a promising tool for H_2S_2-related pathological research and future H_2S_2 probe development [98].

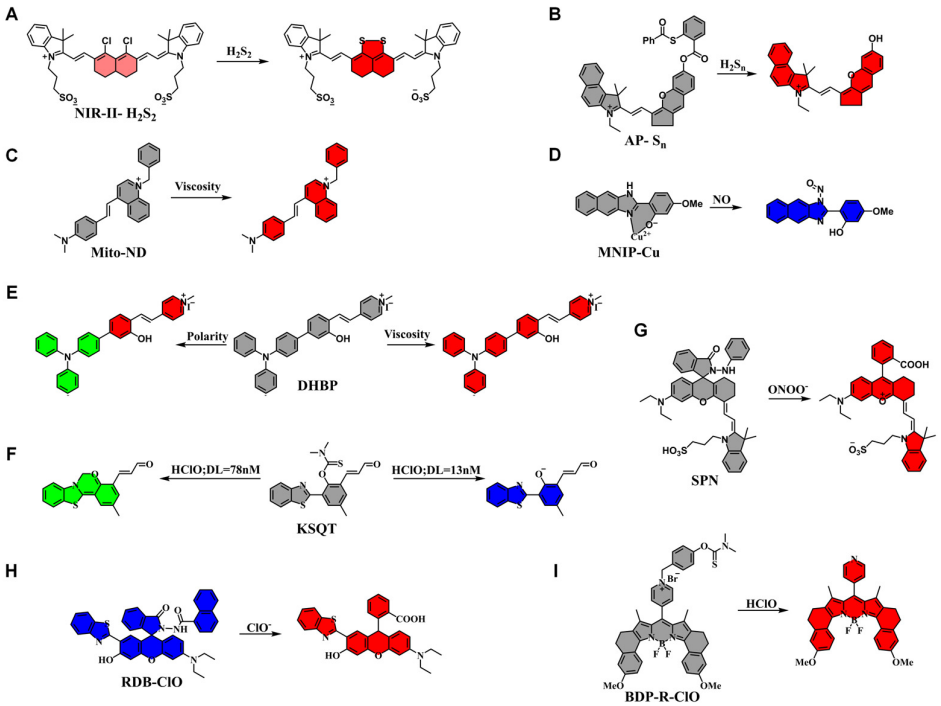


Figure 14. (**A–I**) Structure and detection mechanism of fluorescent probe in LPS-induced liver injury models.

Zhao et al. synthesized AP-Sn, an H_2Sn-activated photoacoustic probe, utilizing semi-anthocyanidin dye as the core structure and phenyl-2-(benzoylthio)benzoic acid as the

reactive moiety (Figure 14B). H_2Sn, a key oxidation product of H_2S, plays a fundamental role in ion channel signaling and tumor suppression, while its dysregulation is associated with various inflammatory diseases. AP-Sn exhibits high stability, excellent biocompatibility, and high specificity for H_2S_4, making it a powerful tool for real-time monitoring of LPS-induced liver injury progression. This probe provides an advanced platform for in situ imaging and mechanistic studies of ALI [99].

Lin et al. designed Mito-ND, a viscosity-sensitive near-infrared fluorescent probe with mitochondrial localization, excellent chemical stability, and photostability (Figure 14C). Mito-ND enables fluorescence imaging of viscosity changes in vitro and successfully detected viscosity alterations in LPS-induced liver injury in mice, demonstrating its potential for clinical liver and kidney disease research (Figure 15) [100].

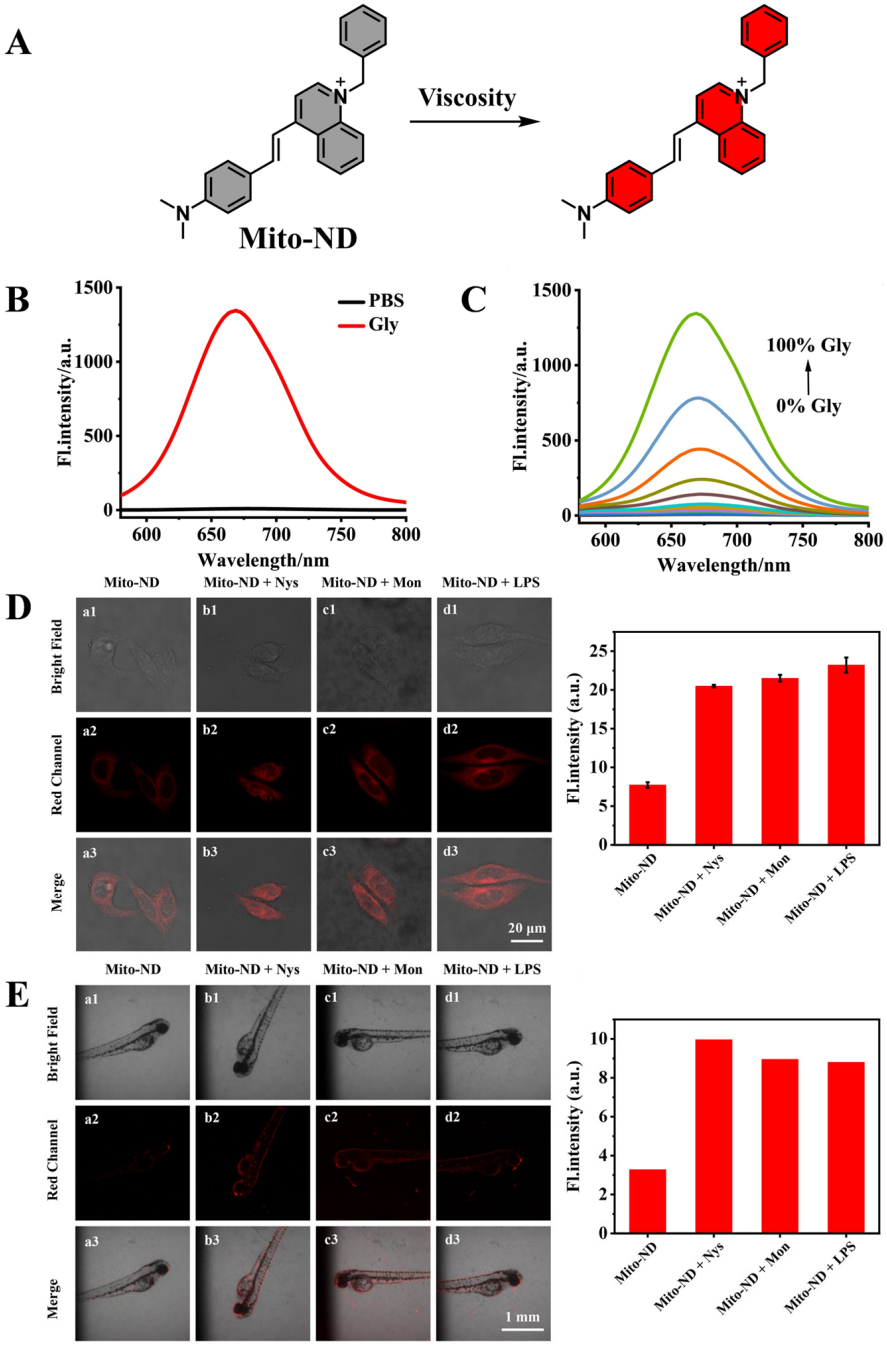


Figure 15. (**A**) Viscosity response mechanism of the fluorescent probe Mito-ND. (**B**) fluorescence spectra of Mito-ND (10 μM) in PBS and glycerol solution. (**C**) Fluorescence spectra of Mito-ND (10 μM)

in PBS-glycerol solution with different viscosity (1.5 cp-1099.5 cp). (**D**) Confocal fluorescence images and fluorescence intensities of HeLa cells incubated with Mito-ND (10 μM) only, and pretreated with different reagents (20 μM Nys, 20 μM Mon, or 20 μg/mL LPS) for 20 min and then incubated with Mito-ND (10 μM) for another 20 min (**a1**,**b1**,**c1**,**d1**) Bright field. (**a2**,**b2**,**c2**,**d2**) Fluorescence field. (**a3**,**b3**,**c3**,**d3**) Merge field. Scale bar: 20 μm (**E**) Confocal fluorescence images and fluorescence intensities of zebrafish incubated with Mito-ND (10 μM) only, and pretreated with different reagents (20 μM Nys, 20 μM Mon, or 20 μg/mL LPS) for 30 min and then incubated with Mito-ND (10 μM) for another 30 min (**a1**,**b1**,**c1**,**d1**) Bright field. (**a2**,**b2**,**c2**,**d2**) Fluorescence field. (**a3**,**b3**,**c3**,**d3**) Merge field. Scale bar: 1 mm. Derived from Ref. [100] with authorization from Copy-right 2022, Elsevier.

Zhang et al. developed MNIP-Cu, a fluorescent probe specifically designed for NO detection, which features rapid binding, high selectivity, and ease of synthesis (Figure 14D). Using MNIP-Cu, researchers successfully visualized and quantified NO distribution in LPS-induced acute liver injury mouse models, demonstrating its potential for biomedical applications in immune liver injury research [101].

Yu et al. synthesized DHBP, a dual-functional fluorescent probe capable of detecting microenvironmental viscosity and polarity fluctuations induced by LPS exposure (Figure 14E). DHBP was successfully applied to LPS-induced liver injury models, demonstrating its potential as a diagnostic tool for immune liver injury studies [102].

Guo et al. developed KSQT, a small-molecule fluorescent probe based on an HBT-derived scaffold, designed for real-time, dual-mode HOCl monitoring (Figure 14F). KSQT enables on/off fluorescence switching and ratiometric response for HOCl detection. Live-cell and zebrafish imaging demonstrated the probe's ability to track both exogenous and endogenous HOCl in real time, making it a powerful tool for high-resolution in vivo imaging of HOCl-related processes [103].

Xu et al. developed SPN, a phenylhydrazine-based near-infrared fluorescent probe, optimized for $ONOO^-$ detection (Figure 14G). SPN exhibits low detection limits, high sensitivity, and excellent water solubility, making it suitable for cellular and in vivo imaging. It successfully detected $ONOO^-$ in LPS-induced zebrafish liver injury models, confirming its utility in diagnosing immune liver injury and evaluating therapeutic interventions (Figure 16) [104].

Hou et al. developed RDB-ClO, a rhodamine-based fluorescent probe for ClO^- detection, featuring high selectivity, low detection limits, rapid response, and high sensitivity (Figure 14H). The probe effectively tracked endogenous and exogenous ClO^- in live cells and zebrafish models and was successfully applied to detect ClO^- fluctuations in E. coli and LPS-induced liver injury models. These findings highlight RDB-ClO's potential as a powerful tool for exploring disease pathogenesis and studying antimicrobial drug effects [105].

Zhao et al. synthesized BDP-R-ClO, a HOCl-responsive fluorescent probe incorporating benzothiazole coumarin and hydroxycoumarin via a piperazine linker (Figure 14I). The probe demonstrated high specificity, rapid response, and broad pH adaptability. BDP-R-ClO was effectively applied to cellular imaging and in vivo imaging of LPS-induced liver injury models, confirming its potential as a diagnostic tool for immune liver injury research [106].

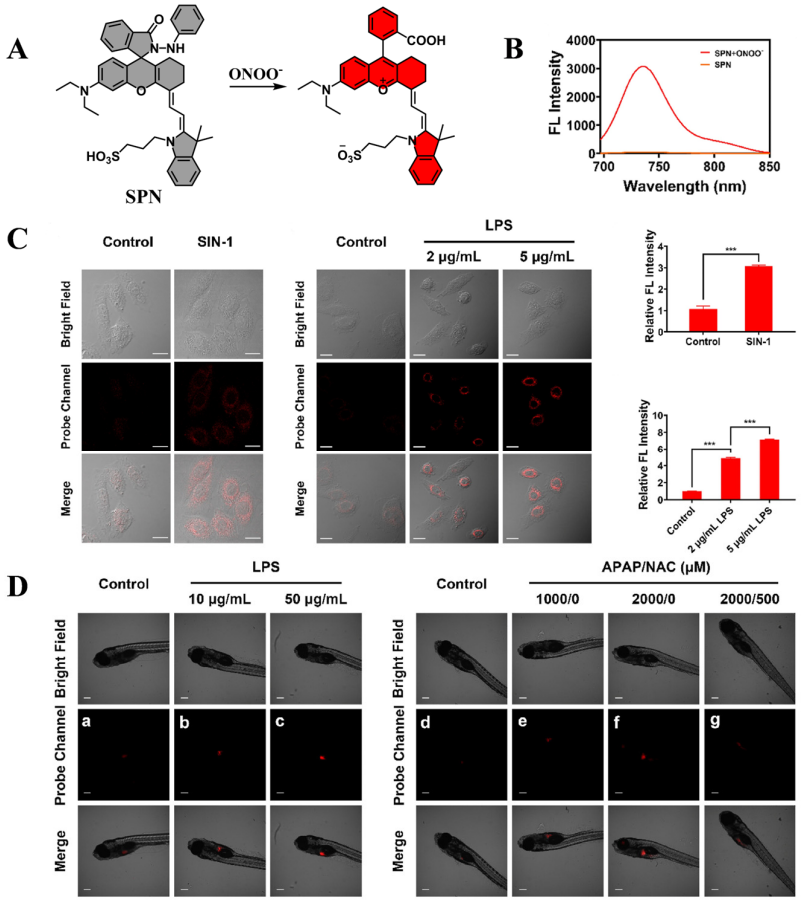


Figure 16. (**A**) $ONOO^-$ response mechanism of the fluorescent probe SPN. (**B**) Fluorescence spectra of SPN with $ONOO^-$. (**C**) Fluorescence imaging and relative fluorescence intensity of exogenous and endogenous $ONOO^-$ in HepG2 cells. Scale bar: 20 μm. Error bars are ± SD (n = 3). Statistical significance levels: *** $p < 0.001$. (**D**) In vivo imaging of LPS/APAP-induced liver injury in zebrafish. Scale bar: 200 μm. Derived from Ref. [104] with authorization from Copyright 2023, Elsevier.

5.3. D-GalN/LPS-Induced Liver Injury Models

D-GalN is a well-established sensitizer of LPS that significantly amplifies the hepatotoxic effects of LPS [108,109]. The combined administration of D-GalN and LPS leads to severe hepatic necrosis and inflammation, making this model a widely used tool for studying ILI.

D-GalN exerts its hepatotoxic effects through multiple mechanisms. Upon entering the body, D-GalN reacts with UDP to form UDP-galactosamine, which leads to rapid depletion of UDP. Since UDP is essential for the biosynthesis of nucleic acids, glycoproteins, and lipopolysaccharides, prolonged UDP depletion severely disrupts cellular metabolism and detoxification processes, further aggravating hepatic damage. Moreover, D-GalN triggers ROS production, inducing severe lipid peroxidation in hepatocyte membranes and initiating oxidative stress-induced apoptosis.

Hepatocyte apoptosis occurs via three main pathways: the death receptor (extrinsic) pathway, the mitochondrial (intrinsic) pathway, and the endoplasmic reticulum stress-induced pathway. Under pathological conditions, these three pathways form a cascading apoptotic response, leading to DNA fragmentation and cytoskeletal protein degradation, ultimately resulting in cell death. Meanwhile, LPS activates hepatic macrophages (Kupffer cells), stimulating the secretion of proinflammatory cytokines such as TNF-α, IL-6, and IL-1β, thereby exacerbating hepatic necrosis and disrupting antioxidant enzyme homeostasis. The synergistic hepatotoxicity of D-GalN and LPS creates a highly specific

liver-targeted immune response, which is widely utilized in experimental models of acute liver failure [110,111].

D-GalN/LPS co-administration induces specialized hepatic macrophage activation, which plays a pivotal role in host immune defense. Kupffer cells secrete proinflammatory cytokines (TNF-α, IL-6, IL-1β) and ROS, triggering NF-κB and p38 MAPK activation, leading to the upregulation of multiple cytokine synthesis pathways. Furthermore, this model induces organelle-specific stress, including endoplasmic reticulum stress, while impairing the mitochondrial ROS defense network, ultimately inhibiting antioxidant enzyme production and worsening hepatic damage [112–114].

Wan et al. used male mice, injecting them intraperitoneally with 10 μg/kg of LPS and 700 mg/kg of D-GalN, followed by sacrificing the animals 5 h later to collect serum, liver, and spleen samples [115]. Qu et al. developed a similar model using C57BL/6 mice, dissolving D-GalN/LPS in phosphate-buffered saline and injecting 30 μg/kg of LPS and 600 mg/kg of D-GalN intraperitoneally. Mice were euthanized 6 h post-injection using 2% sodium pentobarbital, and blood samples were collected via orbital puncture (Figure 17) [116]. Feng et al. used BALB/c mice, administering 10 μg/kg of LPS and 700 mg/kg of D-GalN intraperitoneally, establishing a liver injury model within 6 h [117].

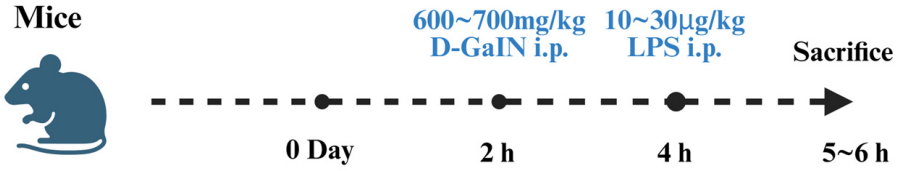


Figure 17. Schematic representation of D-GalN/LPS-induced liver injury in animal models.

The D-GalN/LPS model is highly efficient due to its ability to induce acute liver injury with low LPS doses. As a potent LPS sensitizer, D-GalN enhances LPS hepatotoxicity by several orders of magnitude, allowing researchers to induce acute liver failure with minimal LPS exposure. This model closely resembles human infectious liver injury, making it an ideal tool for studying the pathogenesis of acute liver injury, as well as for screening therapeutic agents with hepatoprotective effects against infection-induced liver damage. Meanwhile a large number of fluorescent probes for the detection of D-GalN/LPS-induced liver injury already exist (Table 5).

Table 5. Characterization of fluorescent probes in D-GalN/LPS-Induced Liver Injury.

Compounds	Trigger	λex (nm)	λem (nm)	Ref.
DMOPB	NO	574	622	[118]
MBTD	NO	421	625/550	[119]
Nil-ClO	HClO/ClO^-	560	650	[120]
PTZCy	ClO^-	625	700/820	[121]
S-BODIPY	ClO^-	540	587/619	[122]
TMSDNPOB	H_2S	574	592	[123]
Cou-dhz-Ph-NO_2	OCl^-	430	478	[124]
Hcy-Biot	$O_2^{\bullet-}$ H_2Sn	730 730	780 780	[125]
DMONPB	H_2S	576	627	[126]

5.4. Application of Fluorescent Probes in D-GalN/LPS-Induced Liver Injury

Wang et al. developed DMOPB, a BODIPY-based fluorescent probe designed for NO detection (Figure 18A). The probe exhibits high sensitivity, strong selectivity, low toxicity, and minimal background fluorescence, enabling precise visualization of NO in cells and tissues. By expanding the Stokes shift, DMOPB enhances NO detection capabilities and has been successfully applied to D-GalN/LPS-induced liver injury models. These findings demonstrate that BODIPY-based fluorescent probes provide a powerful tool for NO imaging in immune liver injury studies [118].

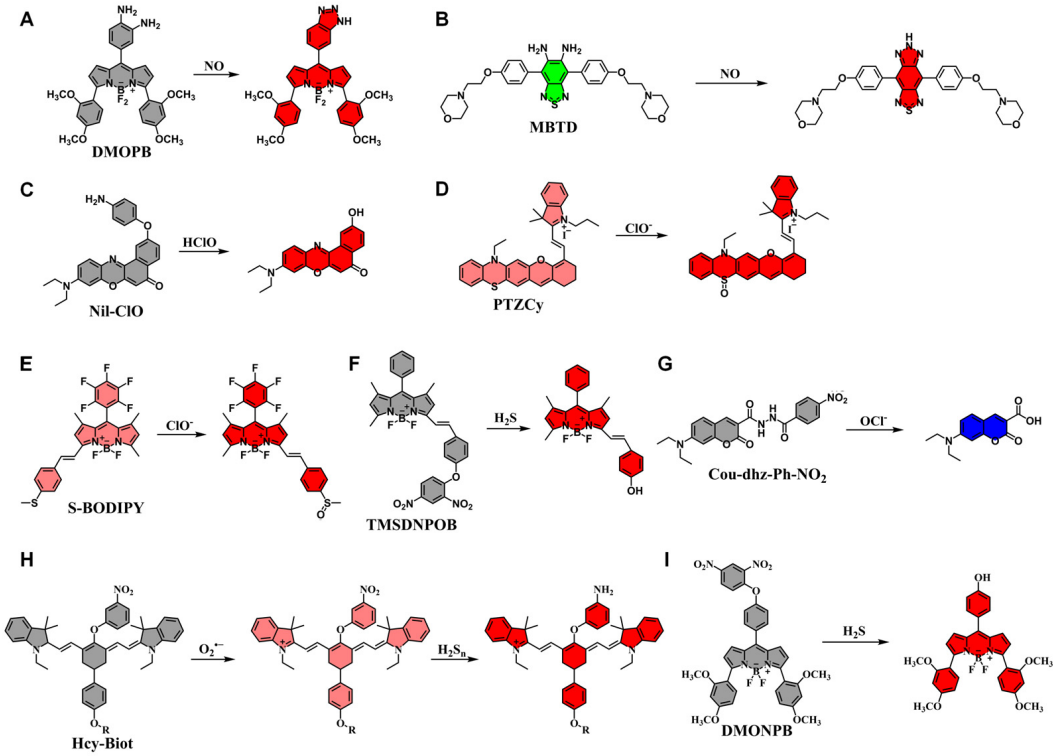


Figure 18. (**A–I**) Structure and detection mechanism of fluorescent probe in D-GalN/LPS-induced liverinjury models.

Ding et al. synthesized MBTD, a dual-intramolecular charge transfer fluorescent probe, which incorporates an OPD fragment into a donor-acceptor-donor fluorophore, allowing for far-red emission and NO detection (Figure 18B). MBTD exhibits a large fluorescence on-off ratio, long fluorescence lifetime, high photostability, and excellent specificity for NO. Notably, MBTD is lysosome-compatible, making it suitable for specific imaging of lysosomal NO levels. In D-GalN/LPS-induced liver injury models, MBTD effectively monitored NO fluctuations in lysosomes, revealing the key role of inducible nitric oxide synthase in NO production during hepatic inflammation. These findings suggest that NO serves as a crucial biomarker for acute liver injury, and MBTD represents a valuable tool for precise NO detection in lysosomal environments [119].

Kong et al. designed Nil-ClO, a two-photon near-infrared fluorescent probe derived from Nile Red, capable of selective HClO/ClO^- detection (Figure 18C). Nil-ClO exhibits high stability, excellent selectivity, and deep tissue penetration, enabling in vivo imaging of HClO/ClO^- in D-GalN/LPS-induced liver injury models. This probe serves as an effective molecular tool for investigating the role of HClO/ClO^- in immune-mediated hepatic inflammation [120].

Xu et al. synthesized PTZCy, a benzothiazole-semicyanine-based ratiometric fluorescent probe for ClO^- detection. PTZCy responds rapidly and selectively to ClO^-, facilitating

the real-time monitoring of endogenous and exogenous ClO^- fluctuations in D-GalN/LPS-induced liver injury models (Figures 18D and 19). These results highlight PTZCy as a promising tool for early-stage liver injury diagnosis and in vivo ClO^- imaging [121].

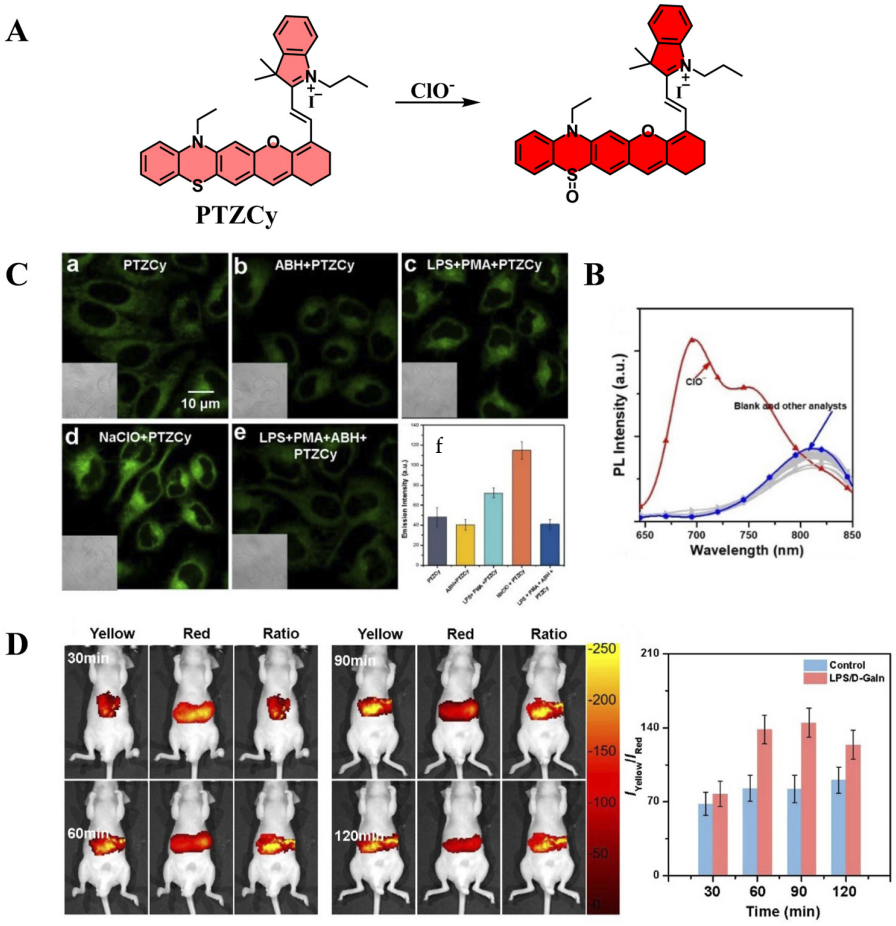


Figure 19. (**A**) OCl^- response mechanism of the fluorescent probe PTZCy. (**B**) Emission spectra of PTZCy (5 μM) with the increasing OCl^- concentrations (0–150 μM) in EtOH/PBS buffer. (**C**) Confocal fluorescence images and fluorescence intensity of the probe in RAW264.7 cells under different conditions. (**a**–**e**) PTZCy group: cells were incubated with PTZCy (5 μM, 30 min), then imaged; ABH+PTZCy group: cells were pretreated with ABH (250 μM, 4 h), next incubated with PTZCy (5 μM, 30 min), then imaged; LPS/PMA+PTZCy group: cells were treated with LPS (5 $\mu g \cdot mL^{-1}$) and PMA (5 $\mu g \cdot mL^{-1}$) for 12 h, then incubated with PTZCy (5 μM, 30 min) and imaged; NaClO+PTZCy group: cells were treated with NaClO (200 μM, 4 h), then incubated with PTZCy (5 μM, 30 min) and imaged; LPS/PMA+ABH+PTZCy group: cells were treated with LPS (5 $\mu g \cdot mL^{-1}$) and PMA (5 $\mu g \cdot mL^{-1}$) for 12 h, then treated with ABH (250 μM, 4 h), finally incubated with PTZCy (5 μM, 30 min) and imaged. Scale bar: 10 μm. (λex = 633 nm, λem = 650–780 nm). (**f**) Intensity of green fluorescence obtained in the above five groups, data = mean ± S.D., n = 3. (**D**) In vivo imaging and fluorescence intensity ratio of mice treated with LPS/D-GalN at different times, I.V. injected with PTZCy. (λex = 620 nm, yellow channel: λem = 650–780 nm, red channel: λem = 790–850 nm). Data = mean ± S.D., n = 3. Derived from Ref. [121] with authorization from Copyright 2024, Elsevier.

Kim et al. developed S-BODIPY, a BODIPY-based ratiometric fluorescent probe for HClO/ClO^- detection, enabling real-time imaging of ClO^- both in vitro and in vivo (Figure 18E). S-BODIPY exhibits high fluorescence quantum yield, strong pH stability, good membrane permeability, and excellent biocompatibility, making it well-suited for tracking ClO^- fluctuations in D-GalN/LPS-induced liver injury models (Figure 20). These results demonstrate the potential of S-BODIPY as an efficient tool for ClO^- detection in hepatic inflammation research [122].

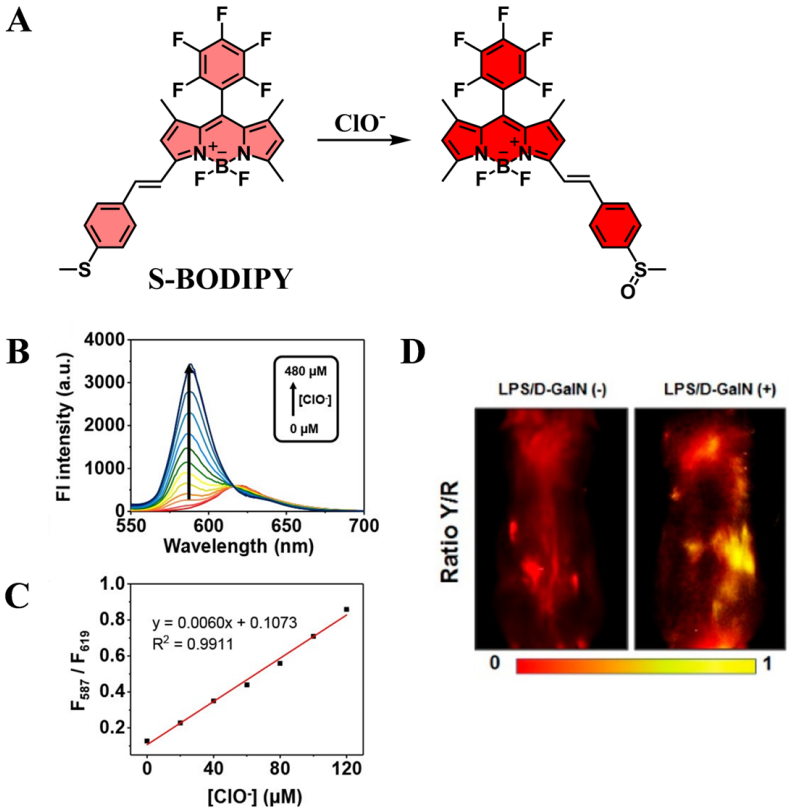


Figure 20. (**A**) ClO^- response mechanism of the fluorescent probe S-BODIPY. (**B**) Fluorescence spectral changes of S-BODIPY (5 μM) in DMF/PBS solution (v/v = 1/1, pH 7.4, 10 mM) upon addition of increasing amounts of NaClO (0–480 μM). Each spectrum was recorded after 1 min. (**C**) Linear relationships between fluorescence intensity ratios (F587/F619) of S-BODIPY (5 μM) versus concentrations of NaClO. (**D**) In vivo imaging of endogenous HClO production from the peritoneal cavity of the mice treated with LPS/D-GalN. Representative images of mice intravenously treated with S-BODIPY (1 mM) for 2 h, pretreated via intraperitoneal injection of PBS (left) and LPS/D-GalN (right). Ratiometric fluorescence images of mice (λex = 550 nm, yellow channel (λem = 550–610 nm) and red channel (λem = 610–670 nm)). Derived from Ref. [122] with authorization from Copyright 2019, American Chemical Society.

Wang et al. designed TMSDNPOB, a dinitrophenyl ether-based fluorescent probe capable of detecting H_2S via thiolysis reactions (Figure 18F). The probe exhibits long-wavelength fluorescence, minimal background interference, and low photodamage, making it suitable for in vivo H_2S imaging. TMSDNPOB enables real-time visualization of both exogenous and endogenous H_2S in D-GalN/LPS-induced liver injury models, confirming its high sensitivity, biocompatibility, and selectivity [123].

Mo et al. synthesized Cou-dhz-Ph-NO_2, a coumarin-based fluorescent probe incorporating aromatic dihydrazines as the linking unit (Figure 18G). The probe exhibits high specificity, rapid response kinetics, and low background fluorescence, facilitating sensitive OCl^- detection. Cou-dhz-Ph-NO_2 successfully visualized OCl^- dynamics in living cells and monitored OCl^- fluctuations in acute liver injury models, demonstrating its potential as a diagnostic tool for OCl^- related liver diseases [124].

Chen et al. developed Hcy-Mito and Hcy-Biot, two near-infrared fluorescent probes designed for simultaneous $O_2^{\bullet-}$ and H_2Sn detection (Figure 18H). These probes exhibit high sensitivity, deep tissue penetration, and strong selectivity, enabling real-time imaging of $O_2^{\bullet-}$ and H_2Sn in D-GalN/LPS-induced liver injury models. Their application in ex vivo and in vivo imaging highlights their potential as valuable tools for investigating oxidative stress and sulfur metabolism in immune liver injury [125].

Wang et al. synthesized DMONPB, a BODIPY-based fluorescent probe with a large Stokes shift, specifically designed for H_2S detection (Figure 18I). The probe exhibits strong photostability, pH insensitivity, low cytotoxicity, and high selectivity for H_2S, making it highly suitable for cellular and tissue imaging. DMONPB was successfully applied to D-GalN/LPS-induced liver injury models, providing an effective method for visualizing H_2S dynamics in immune liver injury research [126].

6. Conclusions

This review systematically summarizes the mechanisms and modeling methods of various liver injury models used in experimental studies, as well as the latest advances in fluorescent probe technology developed for liver injury detection. Liver injury is an intrinsically complex pathological process, and traditional diagnostic methods often suffer from limitations such as low sensitivity, time-consuming procedures, and invasive sample collection. In contrast, fluorescent probes have emerged as powerful analytical tools due to their rapid response, simplicity, and high sensitivity. Recent breakthroughs in fluorescent probe technology have significantly enhanced its applications in liver injury detection, particularly in target identification, localization of injury sites, and quantitative assessment of lesion severity. These advancements have not only provided valuable visualization tools for liver disease research but also established a foundation for early intervention and personalized therapeutic strategies.

Despite the distinct etiologies of alcoholic, chemical, drug-induced, and immune-mediated liver injuries, they share common pathological features such as oxidative stress, inflammatory cytokine release, and hepatocyte apoptosis. Key molecular markers, including ROS and TNF-α, play a central role in multiple liver injury mechanisms, making them universal targets for fluorescent probe development. However, the variability in oxidative stress intensity and biomarker profiles across different liver injury models highlights the need for highly specific and ultrasensitive fluorescent probes capable of dynamic detection and cross-model analysis.

While significant progress has been made in the field of fluorescent probe design, several challenges remain. Most existing probes are designed to detect a single biomarker, whereas liver injury is typically characterized by the interplay of multiple biomolecules and enzymes. This necessitates the development of dual- or multi-target fluorescent probes, which will likely become the future direction in the field. However, the potential for signal interference between multiple fluorophores in multiplexed probes must be carefully addressed to ensure detection accuracy and reliability. Therefore, future research should focus on optimizing key probe properties, including photostability, biocompatibility, low toxicity, high selectivity, and ultra-high sensitivity, while simultaneously advancing multifunctional, synergistic detection strategies.

Another critical challenge is the limited tissue penetration depth of fluorescence imaging, which currently restricts its application to small animal models or ex vivo human liver tissues. To enable non-invasive, real-time diagnosis in clinical settings, the development of NIR-II fluorescent probes has gained significant attention. These NIR-II probes offer deeper tissue penetration, reduced background interference, and enhanced imaging resolution, potentially overcoming the constraints of conventional fluorescence imaging.

Future advancements in fluorescent probe technology will also benefit from interdisciplinary integration with other cutting-edge approaches, further enhancing the precision and efficacy of liver disease diagnosis and therapy. For instance, combining fluorescent probes with nanomaterials could enable simultaneous imaging, quantitative assessment, and targeted drug delivery to the site of liver injury. Additionally, emerging therapeutic modalities such as PDT and PTT have demonstrated promising potential for liver disease

treatment, yet their clinical applicability remains limited by poor tissue penetration and suboptimal cell targeting. The integration of fluorescent probes with PDT and PTT could significantly enhance their spatial precision and therapeutic efficiency, broadening their clinical applications.

In summary, fluorescent probes hold immense potential for advancing liver injury detection, early diagnosis, and personalized medicine. Their continued development will not only deepen our understanding of liver disease pathophysiology but also provide critical support for precision medicine and targeted therapeutic strategies. The pursuit of more efficient, multifunctional, and clinically translatable fluorescent probes will have a profound impact on elucidating liver injury mechanisms and accelerating innovations in liver disease diagnostics and therapeutics.

Author Contributions: Writing—original draft preparation, S.L.; software, F.H.; investigation, F.Z.; supervision, X.H.; visualization, J.Z.; supervision, D.P.; funding acquisition, J.H. All authors have read and agreed to the published version of the manuscript.

Funding: This work was financed by Science and Technology program of Gansu Province (24JRRA063), Yunnan Province Major Scientific and Technological Project (202302AE090007 and 202402AA310034), Key R&D Program of Yunnan Province (202203AD150003), Gansu Science Fund for Basic Creative Research Groups (25JRRA469), Gansu Province Intellectual Property Plan Project (23ZSCQG026), Key Research and Development Program of Sichuan Province (2023YFS0339).

Institutional Review Board Statement: Not Applicable.

Informed Consent Statement: Not Applicable.

Data Availability Statement: Not Applicable.

Conflicts of Interest: The authors declare no conflicts of interest.

Abbreviations

The following abbreviations are used in this manuscript:

ALI	Alcoholic liver injury
CLI	Chronic liver injury
AALI	Acute alcoholic liver injury
DILI	Drug-induced liver injury
ILI	Immune-mediated liver injury
ALD	Alcoholic liver disease
CCl_4	Carbon tetrachloride
APAP	Acetaminophen
D-GalN	D-galactosamine
LPS	Lipopolysaccharide
AST	Aspartate aminotransferase
ALT	Alanine aminotransferase
ROS	Reactive oxygen species
RNS	Reactive nitrogen species
CYP450	Cytochrome P450
HClO	Hypochlorous acid
$O_2^{\bullet-}$	Superoxide anions
Cys	Cysteine
NO	Nitric oxide
GSTs	Glutathione S-transferase
H_2S_2	Hydrogen persulfide
H_2O_2	Hydrogen peroxide
GSH	Glutathione

$ONOO^-$	Peroxynitrite
IL-1β	Interleukin-1β
IL-1	Interleukin-1
IL-6	Interleukin-6
TNF-α	Tumor necrosis factor-alpha
IL-1RA	Interleukin-1 receptor antagonist
NF-κB	Nuclear factor-kappa B
NAFLD	Non-alcoholic fatty liver disease
AIE	Aggregation-induced emission
NIR-II	Near-infrared second-window
UDP	Uridine diphosphate
NAPQI	N-acetyl-p-benzoquinoneimine
H&E	Hematoxylin and eosin
PDT	Photodynamic therapy
PTT	Photothermal therapy

References

1. Trefts, E.; Gannon, M.; Wasserman, D.H. The liver. *Curr. Biol.* **2017**, *27*, R1147–R1151. [CrossRef] [PubMed]
2. Damm, T.W.; Kramer, D.J. The Liver in Critical Illness. *Crit. Care Clin.* **2016**, *32*, 425–438. [CrossRef] [PubMed]
3. Crabb, D.W.; Im, G.Y.; Szabo, G.; Mellinger, J.L.; Lucey, M.R. Diagnosis and Treatment of Alcohol-Associated Liver Diseases: 2019 Practice Guidance From the American Association for the Study of Liver Diseases. *Hepatology* **2020**, *71*, 306–333. [CrossRef]
4. Zhang, Y.; Lu, Y.; Ji, H.; Li, Y. Anti-inflammatory, anti-oxidative stress and novel therapeutic targets for cholestatic liver injury. *Biosci. Trends* **2019**, *13*, 23–31. [CrossRef]
5. Duarte, S.; Baber, J.; Fujii, T.; Coito, A.J. Matrix metalloproteinases in liver injury, repair and fibrosis. *Matrix Biol.* **2015**, *44–46*, 147–156. [CrossRef]
6. Giordano, C.M.; Zervos, X.B. Clinical manifestations and treatment of drug-induced hepatotoxicity. *Clin. Liver Dis.* **2013**, *17*, 565–573. [CrossRef]
7. Thomson, J.; Hargrove, L.; Kennedy, L.; Demieville, J.; Francis, H. Cellular crosstalk during cholestatic liver injury. *Liver Res.* **2017**, *1*, 26–33. [CrossRef]
8. Guicciardi, M.E.; Gores, G.J. Apoptosis: A mechanism of acute and chronic liver injury. *Gut* **2005**, *54*, 1024–1033. [CrossRef]
9. Ozer, J.; Ratner, M.; Shaw, M.; Bailey, W.; Schomaker, S. The current state of serum biomarkers of hepatotoxicity. *Toxicology* **2008**, *245*, 194–205. [CrossRef]
10. Ueno, T.; Nagano, T. Fluorescent probes for sensing and imaging. *Nat. Methods* **2011**, *8*, 642–645. [CrossRef]
11. Huang, J.; Pu, K. Activatable Molecular Probes for Second Near-Infrared Fluorescence, Chemiluminescence, and Photoacoustic Imaging. *Angew. Chem. Int. Engl.* **2020**, *59*, 11717–11731. [CrossRef] [PubMed]
12. Shuhendler, A.J.; Pu, K.; Cui, L.; Uetrecht, J.P.; Rao, J. Real-time imaging of oxidative and nitrosative stress in the liver of live animals for drug-toxicity testing. *Nat. Biotechnol.* **2014**, *32*, 373–380. [CrossRef] [PubMed]
13. Zhou, Y.; Yang, X.; Wei, X.; Zhang, S.-S.; Yan, M. Recent progress in small molecule fluorescent probes for imaging and diagnosis of non-alcoholic fatty liver disease. *Coord. Chem. Rev.* **2024**, *513*, 215864. [CrossRef]
14. Li, Z.-J.; Wang, C.-Y.; Xu, L.; Zhang, Z.-Y.; Tang, Y.-H.; Qin, T.-Y.; Wang, Y.-L. Recent Progress of Activity-Based Fluorescent Probes for Imaging Leucine Aminopeptidase. *Biosensors* **2023**, *13*, 752. [CrossRef]
15. Liu, X.; Yu, S.; Zhang, Y.; Zhang, W.; Zhong, H.; Lu, X.; Guan, R. A review on the protective effect of active components in Antrodia camphorata against alcoholic liver injury. *J. Ethnopharmacol.* **2023**, *300*, 115740. [CrossRef]
16. Meier, P.; Seitz, H.K. Age, alcohol metabolism and liver disease. *Curr. Opin. Clin. Nutr. Metab. Care* **2008**, *11*, 21–26. [CrossRef]
17. Jones, B.E.; Liu, H.; Lo, C.R.; Koop, D.R.; Czaja, M.J. Cytochrome P450 2E1 expression induces hepatocyte resistance to cell death from oxidative stress. *Antioxid. Redox Signal.* **2002**, *4*, 701–709. [CrossRef]
18. Yu, S.; Rao, S.; Reddy, J.K. Peroxisome proliferator-activated receptors, fatty acid oxidation, steatohepatitis and hepatocarcinogenesis. *Curr. Mol. Med.* **2003**, *3*, 561–572. [CrossRef]
19. Lieber, C.S. Alcoholic fatty liver: Its pathogenesis and mechanism of progression to inflammation and fibrosis. *Alcohol* **2004**, *34*, 9–19. [CrossRef]
20. Tuma, D.J.; Casey, C.A. Dangerous byproducts of alcohol breakdown--focus on adducts. *Alcohol Res. Health* **2003**, *27*, 285–290.
21. Miranda-Mendez, A.; Lugo-Baruqui, A.; Armendariz-Borunda, J. Molecular basis and current treatment for alcoholic liver disease. *Int. J. Environ. Res. Public Health* **2010**, *7*, 1872–1888. [CrossRef] [PubMed]
22. Ma, Y.; Wang, D.; Xu, X.; Yang, X.; Wang, X.; Zhu, Z.; Zhao, Y.; Chen, M.; Xu, F.; Fu, L.; et al. Dynamic changes of ROS, MDA and SOD during arsenic-induced neoplastic transformation in human keratinocytes. *J. Hyg. Res.* **2015**, *44*, 456–461.

23. Zhao, X.; Xue, X.; Wang, C.; Wang, J.; Peng, C.; Li, Y. Emerging roles of Sirtuins in alleviating alcoholic liver Disease: A comprehensive review. *Int. Immunopharmacol.* **2022**, *108*, 108712. [CrossRef] [PubMed]
24. Chen, J.; Zhang, Q.; Wang, R.; Yang, Y.; Wang, Y.; Liu, X.; Zhang, X.; Qiao, X.; Zhong, G.; Wei, J.; et al. Preliminary study on the effective site and mechanism of action of Meconopsis quintuplinervia Regel in alleviating acute alcoholic liver injury in mice. *Int. Immunopharmacol.* **2023**, *308*, 116230. [CrossRef]
25. Liu, X.; Hou, R.; Yan, J.; Xu, K.; Wu, X.; Lin, W.; Zheng, M.; Fu, J. Purification and characterization of Inonotus hispidus exopolysaccharide and its protective effect on acute alcoholic liver injury in mice. *Int. J. Biol. Macromol.* **2019**, *129*, 41–49. [CrossRef]
26. Wang, J.W.; Chen, X.Y.; Hu, P.Y.; Tan, M.M.; Tang, X.G.; Huang, M.C.; Lou, Z.H. Effects of Linderae radix extracts on a rat model of alcoholic liver injury. *Exp. Ther. Med.* **2016**, *11*, 2185–2192. [CrossRef]
27. Song, M.; Chen, T.; Prough, R.A.; Cave, M.C.; McClain, C.J. Chronic Alcohol Consumption Causes Liver Injury in High-Fructose-Fed Male Mice Through Enhanced Hepatic Inflammatory Response. *Alcohol. Clin. Exp. Res.* **2016**, *40*, 518–528. [CrossRef]
28. Tan, X.; Hong, J.; Jiang, S.; Zhang, S.; Chen, Y.; Feng, G. Near-Infrared Fluorescent Probe Reveals Elevated Mitochondrial Viscosity during Acute Alcoholic Liver Injury. *Anal. Chem.* **2024**, *96*, 14860–14866. [CrossRef]
29. Chen, J.; Fang, Y.; Sun, L.; Zeng, F.; Wu, S. An activatable probe for detecting alcoholic liver injury via multispectral optoacoustic tomography and fluorescence imaging. *Chem. Commun.* **2020**, *56*, 11102–11105. [CrossRef]
30. Shen, L.; Ma, M.; Zhou, K.; Jin, M.; Wang, S.; Liu, H.; Yang, Y. Cysteine triggered cascade reaction forming coumarin: Visualization of cysteine fluctuation in alcoholic liver disease by a NIR fluorescent probe. *Spectrochim. Acta Part A Mol. Biomol. Spectrosc.* **2025**, *324*, 124974. [CrossRef]
31. Ma, X.; Han, R.; Wang, J.; Zhang, B.; Ruan, M.; Zhao, W.; Zhang, J. Novel NIR fluorescent probe based on BODIPY for diagnosis and treatment evaluation of alcoholic liver disease via visualizing HClO fluctuation. *Spectrochim. Acta Part A Mol. Biomol. Spectrosc.* **2025**, *328*, 125497. [CrossRef] [PubMed]
32. Feng, Y.; Nie, G.; Liang, W.; Li, W.; Zhang, Y.; Wang, K.; Chen, D. Real-time imaging of acute alcoholic liver injury in vivo via a robust viscosity probe with aggregation-induced emission nature. *Sens. Actuators B Chem.* **2022**, *355*, 131285. [CrossRef]
33. Wang, S.; Zhao, X.; Liu, M.; Yang, L.; Yu, M.; Li, Z. A dual-responsive crimson fluorescent probe for real-time diagnosis of alcoholic acute liver injury. *Biosens. Bioelectron.* **2023**, *239*, 115596. [CrossRef]
34. Niu, P.; Liu, J.; Xu, F.; Yang, L.; Li, Y.; Sun, A.; Wei, L.; Liu, X.; Song, X. Dual-Ratiometric Fluorescent Probe for H2O2 and HClO in Living Cells and Zebrafish and Application in Alcoholic Liver Injury Monitoring. *ACS Appl. Bio Mater.* **2022**, *5*, 1683–1691. [CrossRef]
35. Zhang, B.; Qin, S.; Wang, J.; Ma, X.; Han, R.; Ruan, M.; Zhao, W.; Zhang, J. A near-infrared $ONOO^-$-activated fluorescent probe for real-time visualizing of alcoholic liver disease. *J. Mol. Struct.* **2025**, *1323*, 140805. [CrossRef]
36. Wang, R.; Zhou, X.; Li, B.; Ding, R.; Han, J.; Wang, Y.; Meng, A.; Zhou, J. A novel dual near-infrared fluorescent probe for bioimaging and visualization of viscosity in acute alcoholic liver injury. *Chem. Commun.* **2024**, *60*, 5804–5807. [CrossRef]
37. Zhang, P.; Wei, L.; Jiang, Q.; Gai, S.; Zhou, Z.; Bian, J.; Zhang, Y.; Han, W.; Shu, W.; He, Y. A turn-on fluorescent probe for detecting and bioimaging of HOCl in inflammatory and liver disease models. *Bioorg. Chem.* **2024**, *143*, 107051. [CrossRef]
38. Lee, Y.S.; Cho, I.J.; Kim, J.W.; Lee, M.K.; Ku, S.K.; Choi, J.S.; Lee, H.J. Hepatoprotective effects of blue honeysuckle on CCl(4)-induced acute liver damaged mice. *Food Sci. Nutr.* **2019**, *7*, 322–338. [CrossRef]
39. Unsal, V.; Cicek, M.; Sabancilar, İ. Toxicity of carbon tetrachloride, free radicals and role of antioxidants. *Rev. Environ. Health* **2021**, *36*, 279–295. [CrossRef]
40. Wang, W.; Jiang, L.; Ren, Y.; Shen, M.; Xie, J. Characterizations and hepatoprotective effect of polysaccharides from Mesona blumes against tetrachloride-induced acute liver injury in mice. *Int. J. Biol. Macromol.* **2019**, *124*, 788–795. [CrossRef]
41. Iwakiri, Y. Nitric oxide in liver fibrosis: The role of inducible nitric oxide synthase. *Clin. Mol. Hepatol.* **2015**, *21*, 319–325. [CrossRef] [PubMed]
42. Li, S.; Liu, J.; Zhang, M.; Chen, Y.; Zhu, T.; Wang, J. Protective Effect of Eckol against Acute Hepatic Injury Induced by Carbon Tetrachloride in Mice. *Mar. Drugs* **2018**, *16*, 300. [CrossRef] [PubMed]
43. Gu, X.; Manautou, J.E. Molecular mechanisms underlying chemical liver injury. *Expert Rev. Mol. Med.* **2012**, *14*, e4. [CrossRef] [PubMed]
44. Badr, G.; Sayed, E.A.; Waly, H.; Hassan, K.A.; Mahmoud, M.H.; Selamoglu, Z. The Therapeutic Mechanisms of Propolis Against CCl(4) -Mediated Liver Injury by Mediating Apoptosis of Activated Hepatic Stellate Cells and Improving the Hepatic Architecture through PI3K/AKT/mTOR, TGF-β/Smad2, Bcl2/BAX/P53 and iNOS Signaling Pathways. *Cell. Physiol. Biochem.* **2019**, *53*, 301–322. [CrossRef]
45. Choi, S.Y.; Song, P.; Hwang, J.S.; Lee, Y.K.; Shin, M.S.; Son, H.J.; Kim, Y.J.; Kim, W.; Lee, K.M. Cereblon deficiency ameliorates carbon tetrachloride-induced acute hepatotoxicity in HepG2 cells by suppressing MAPK-mediated apoptosis. *Front. Immunol.* **2024**, *15*, 1457636. [CrossRef]

46. Salim, N.S.; Abo El-Maati, M.F.; Abdelnour, S.A.; Abdel-Alim, M.E. Hepatoprotective activity of taraxacum officinale extract against CCl4-induced liver injury in rats. *Food Biosci.* **2025**, *68*, 106708. [CrossRef]
47. Lu, Y.; Hu, D.; Ma, S.; Zhao, X.; Wang, S.; Wei, G.; Wang, X.; Wen, A.; Wang, J. Protective effect of wedelolactone against CCl4-induced acute liver injury in mice. *Int. Immunopharmacol.* **2016**, *34*, 44–52. [CrossRef]
48. Lee, M.-M.; Kim, H.-G.; Lee, J.-S.; Lee, S.-B.; Cho, J.-H.; Lee, D.-S.; Lee, N.-H.; Lee, H.-D.; Moon, S.-O.; Son, C.-G. Synergistic hepatoprotective effects of CGplus on CCl4-induced acute injury. *J. Ethnopharmacol.* **2020**, *249*, 112441. [CrossRef]
49. Wang, K.; Guo, R.; Chen, X.-Y.; Li, X.-L.; Hu, Z.-G.; Wang, X.; Wang, C.-Y.; Qin, Y.-J.; Yao, K.; Yang, Y.-S. A novel fluorescent probe for imaging endogenous hydrogen sulfide in living cells and mice models of acute liver injury. *Chem. Eng. J.* **2023**, *468*, 143611. [CrossRef]
50. Zhu, W.; Qian, X.; Wang, J.; Yu, H.; Liu, W.; Wang, H.-Y.; Liu, Y. Near-infrared frequency upconversion probes for monitoring glutathione S-transferase to evaluate acute liver injury. *Sens. Actuators B Chem.* **2021**, *347*, 130640. [CrossRef]
51. Zhou, Y.; Li, P.; Fan, N.; Wang, X.; Liu, X.; Wu, L.; Zhang, W.; Zhang, W.; Ma, C.; Tang, B. In situ visualization of peroxisomal peroxynitrite in the livers of mice with acute liver injury induced by carbon tetrachloride using a new two-photon fluorescent probe. *Chem. Commun.* **2019**, *55*, 6767–6770. [CrossRef] [PubMed]
52. Wang, K.; Guo, R.; Chen, X.-Y.; Yang, Y.-S.; Qiao, L.-Q.; Wang, M.-L. Multifunctional lysosome-targetable fluorescent probe for imaging peroxynitrite in acute liver injury model. *Chem. Eng. J.* **2023**, *455*, 140491. [CrossRef]
53. He, L.; He, L.H.; Xu, S.; Ren, T.B.; Zhang, X.X.; Qin, Z.J.; Zhang, X.B.; Yuan, L. Engineering of Reversible NIR-II Redox-Responsive Fluorescent Probes for Imaging of Inflammation in vivo. *Angew. Chem. Int. Engl.* **2022**, *61*, e202211409. [CrossRef]
54. Hu, Z.-Y.; Chen, X.-Y.; Yang, X.; Li, T.; Yang, Y.-S.; Wang, S.-J.; Wang, K.; Hu, Z.-G. Imaging and detection of sulfite in acute liver injury with a novel quinoxaline-based fluorescent probe. *Anal. Chim. Acta* **2023**, *1261*, 341177. [CrossRef]
55. Meng, T.; Zhang, X.; Tang, W.; Liu, C.; Duan, X. A Small Molecule Chemiluminophore with near 600 nm Emission for In Vivo Imaging of Myeloperoxidase and Inflammatory Diseases. *Chem. Biomed. Imaging* **2024**, *2*, 205–212. [CrossRef]
56. Zhang, T.; Li, Z.; Qin, M.; Zhang, J.; Sun, Y.; Liu, C. Visulization of peroxynitrite variation for accurate diagnosis and assessing treatment response of hepatic fibrosis using a Golgi-targetable ratiometric fluorescent probe. *J. Photochem. Photobiol. B Biol.* **2024**, *257*, 112950. [CrossRef]
57. Yuan, F.; Wang, B.; Hou, J.-T.; Li, J.; Shen, J.; Duan, Y.; Ren, W.X.; Wang, S. Demonstrating HOCl as a potential biomarker for liver fibrosis using a highly sensitive fluorescent probe. *Sens. Actuators B Chem.* **2023**, *378*, 133219. [CrossRef]
58. Garcia-Cortes, M.; Robles-Diaz, M.; Stephens, C.; Ortega-Alonso, A.; Lucena, M.I.; Andrade, R.J. Drug induced liver injury: An update. *Arch. Toxicol.* **2020**, *94*, 3381–3407. [CrossRef]
59. Andrade, R.J.; Chalasani, N.; Björnsson, E.S.; Suzuki, A.; Kullak-Ublick, G.A.; Watkins, P.B.; Devarbhavi, H.; Merz, M.; Lucena, M.I.; Kaplowitz, N.; et al. Drug-induced liver injury. *Nat. Rev. Dis. Primers* **2019**, *5*, 58. [CrossRef]
60. Katarey, D.; Verma, S. Drug-induced liver injury. *Clin. Med.* **2016**, *16*, s104–s109. [CrossRef]
61. Björnsson, H.K.; Björnsson, E.S. Drug-induced liver injury: Pathogenesis, epidemiology, clinical features, and practical management. *Eur. J. Intern. Med.* **2022**, *97*, 26–31. [CrossRef] [PubMed]
62. Wan, M.; Gao, H.; Liu, X.; Zhang, Y. Rutaecarpine Aggravates Acetaminophen-Induced Acute Liver Injury by Inducing CYP1A2. *Toxics* **2024**, *12*, 515. [CrossRef] [PubMed]
63. Hossen, M.S.; Akter, A.; Azmal, M.; Rayhan, M.; Islam, K.S.; Islam, M.M.; Ahmed, S.; Abdullah-Al-Shoeb, M. Unveiling the molecular basis of paracetamol-induced hepatotoxicity: Interaction of N-acetyl-p-benzoquinone imine with mitochondrial succinate dehydrogenase. *Biochem. Biophys. Rep.* **2024**, *38*, 101727. [CrossRef]
64. Hanawa, N.; Shinohara, M.; Saberi, B.; Gaarde, W.A.; Han, D.; Kaplowitz, N. Role of JNK translocation to mitochondria leading to inhibition of mitochondria bioenergetics in acetaminophen-induced liver injury. *J. Biol. Chem.* **2008**, *283*, 13565–13577. [CrossRef]
65. Du, K.; Ramachandran, A.; Weemhoff, J.L.; Chavan, H.; Xie, Y.; Krishnamurthy, P.; Jaeschke, H. Editor's Highlight: Metformin Protects Against Acetaminophen Hepatotoxicity by Attenuation of Mitochondrial Oxidant Stress and Dysfunction. *Toxicol. Sci.* **2016**, *154*, 214–226. [CrossRef]
66. Lee, K.K.; Imaizumi, N.; Chamberland, S.R.; Alder, N.N.; Boelsterli, U.A. Targeting mitochondria with methylene blue protects mice against acetaminophen-induced liver injury. *Hepatology* **2015**, *61*, 326–336. [CrossRef]
67. Jaeschke, H.; Ramachandran, A. Central Mechanisms of Acetaminophen Hepatotoxicity: Mitochondrial Dysfunction by Protein Adducts and Oxidant Stress. *Drug Metab. Dispos.* **2024**, *52*, 712–721. [CrossRef]
68. Wu, Y.; Li, W.; Zhang, J.; Lin, J.; You, L.; Su, J.; Zheng, C.; Gao, Y.; Kong, X.; Sun, X. Shaoyao-Gancao Decoction, a famous Chinese medicine formula, protects against APAP-induced liver injury by promoting autophagy/mitophagy. *Phytomedicine* **2024**, *135*, 156053. [CrossRef]
69. Zhong, Y.H.; Wu, X.W.; Zhang, X.Y.; Zhang, S.W.; Feng, Y.; Zhang, X.M.; Xu, B.B.; Zhong, G.Y.; Huang, H.L.; He, J.W.; et al. Intestinal microbiota-mediated serum pharmacochemistry reveals hepatoprotective metabolites of Platycodonis Radix against APAP-induced liver injury. *J. Chromatogr. B* **2025**, *1251*, 124395. [CrossRef]

70. Lei, P.; Li, X.; Jiang, L.; Yu, H.; Zhang, P.; Han, L.; Jiang, M. Alisma plantago-aquatica polysaccharides ameliorate acetaminophen-induced acute liver injury by regulating hepatic metabolic profiles and modulating gut microbiota. *Int. J. Biol. Macromol.* **2025**, *285*, 138345. [CrossRef]
71. Wu, L.; Liu, J.; Tian, X.; Groleau, R.R.; Bull, S.D.; Li, P.; Tang, B.; James, T.D. Fluorescent probe for the imaging of superoxide and peroxynitrite during drug-induced liver injury. *Chem. Sci.* **2021**, *12*, 3921–3928. [CrossRef] [PubMed]
72. Wu, L.; Liu, J.; Tian, X.; Groleau, R.R.; Feng, B.; Yang, Y.; Sedgwick, A.C.; Han, H.-H.; Wang, Y.; Wang, H.-M.; et al. Dual-Channel Fluorescent Probe for the Simultaneous Monitoring of Peroxynitrite and Adenosine-5′-triphosphate in Cellular Applications. *J. Am. Chem. Soc.* **2022**, *144*, 174–183. [CrossRef] [PubMed]
73. Liu, J.; Li, C.; Sun, J.; Zhang, D.; Yang, X.; Ye, Y.; Zhao, Y. A dual-response fluorescent probe to reveal the role of ferroptosis in drug-induced liver injury. *Chem. Eng. J.* **2024**, *495*, 153592. [CrossRef]
74. Dong, J.; Yang, Y.; Fan, X.; Zhu, H.-L.; Li, Z. Accurate imaging in the processes of formation and inhibition of drug-induced liver injury by an activable fluorescent probe for $ONOO^-$. *Mater. Today Bio* **2023**, *21*, 100689. [CrossRef]
75. Tian, Y.; Liu, S.; Cao, W.; Wu, P.; Chen, Z.; Xiong, H. H_2O_2-Activated NIR-II Fluorescent Probe with a Large Stokes Shift for High-Contrast Imaging in Drug-Induced Liver Injury Mice. *Anal. Chem.* **2022**, *94*, 11321–11328. [CrossRef]
76. Jiao, X.; Xiao, Y.; Li, Y.; Liang, M.; Xie, X.; Wang, X.; Tang, B. Evaluating Drug-Induced Liver Injury and Its Remission via Discrimination and Imaging of HClO and H_2S with a Two-Photon Fluorescent Probe. *Anal. Chem.* **2018**, *90*, 7510–7516. [CrossRef]
77. Shangguan, L.; Wang, J.; Qian, X.; Wu, Y.; Liu, Y. Mitochondria-Targeted Ratiometric Chemdosimeter to Detect Hypochlorite Acid for Monitoring the Drug-Damaged Liver and Kidney. *Anal. Chem.* **2022**, *94*, 11881–11888. [CrossRef]
78. Wang, H.; Liu, C.; He, Z.; Li, P.; Zhang, W.; Zhang, W.; Tang, B. Dual-Colored Fluorescence Imaging of Mitochondrial HNO and Golgi-HNO in Mice with DILI. *Anal. Chem.* **2021**, *93*, 6551–6558. [CrossRef]
79. Liu, L.; Xu, J.; Zhang, S.; Chen, H.; Wang, L.; Shen, X.; Chen, H. Rational design of dual ratiometric photoacoustic and fluorescent probe for reliable imaging and quantitative detection of endogenous CO during drug-induced liver injury and repair. *Sens. Actuators B Chem.* **2022**, *367*, 132171. [CrossRef]
80. Zhang, J.; Jin, Z.; Hu, X.-X.; Meng, H.-M.; Li, J.; Zhang, X.-B.; Liu, H.-W.; Deng, T.; Yao, S.; Feng, L. Efficient Two-Photon Fluorescent Probe for Glutathione S-Transferase Detection and Imaging in Drug-Induced Liver Injury Sample. *Anal. Chem.* **2017**, *89*, 8097–8103. [CrossRef]
81. Kubes, P.; Jenne, C. Immune Responses in the Liver. *Annu. Rev. Immunol.* **2018**, *36*, 247–277. [CrossRef] [PubMed]
82. Polakos, N.K.; Cornejo, J.C.; Murray, D.A.; Wright, K.O.; Treanor, J.J.; Crispe, I.N.; Topham, D.J.; Pierce, R.H. Kupffer cell-dependent hepatitis occurs during influenza infection. *Am. J. Pathol.* **2006**, *168*, 1169–1178. [CrossRef] [PubMed]
83. Santodomingo-Garzon, T.; Swain, M.G. Role of NKT cells in autoimmune liver disease. *Autoimmun. Rev.* **2011**, *10*, 793–800. [CrossRef] [PubMed]
84. Eilat, D. Introduction: Mechanisms of tissue injury in autoimmune diseases. *Semin. Immunopathol.* **2014**, *36*, 491–493. [CrossRef]
85. Gerussi, A.; Natalini, A.; Antonangeli, F.; Mancuso, C.; Agostinetto, E.; Barisani, D.; Di Rosa, F.; Andrade, R.; Invernizzi, P. Immune-Mediated Drug-Induced Liver Injury: Immunogenetics and Experimental Models. *Int. J. Mol. Sci.* **2021**, *22*, 4557. [CrossRef]
86. Xuan, S.; Ma, Y.; Zhou, H.; Gu, S.; Yao, X.; Zeng, X. The implication of dendritic cells in lung diseases: Immunological role of toll-like receptor 4. *Genes Dis.* **2024**, *11*, 101007. [CrossRef]
87. Ciesielska, A.; Matyjek, M.; Kwiatkowska, K. TLR4 and CD14 trafficking and its influence on LPS-induced pro-inflammatory signaling. *Cell. Mol. Life Sci.* **2021**, *78*, 1233–1261. [CrossRef]
88. Giordano, N.P.; Cian, M.B.; Dalebroux, Z.D. Outer Membrane Lipid Secretion and the Innate Immune Response to Gram-Negative Bacteria. *Infect. Immun.* **2020**, *88*, 7. [CrossRef]
89. Wang, J.; Sun, Z.; Xie, J.; Ji, W.; Cui, Y.; Ai, Z.; Liang, G. Inflammasome and pyroptosis in autoimmune liver diseases. *Front. Immunol.* **2023**, *14*, 1150879. [CrossRef]
90. Płóciennikowska, A.; Hromada-Judycka, A.; Borzęcka, K.; Kwiatkowska, K. Co-operation of TLR4 and raft proteins in LPS-induced pro-inflammatory signaling. *Cell. Mol. Life Sci.* **2015**, *72*, 557–581. [CrossRef]
91. Chae, B.S. Pretreatment of Low-Dose and Super-Low-Dose LPS on the Production of In Vitro LPS-Induced Inflammatory Mediators. *Toxicol. Res.* **2018**, *34*, 65–73. [CrossRef] [PubMed]
92. Kawai, T.; Akira, S. Signaling to NF-kappaB by Toll-like receptors. *Trends Mol. Med.* **2007**, *13*, 460–469. [CrossRef] [PubMed]
93. Ntoufa, S.; Vilia, M.G.; Stamatopoulos, K.; Ghia, P.; Muzio, M. Toll-like receptors signaling: A complex network for NF-κB activation in B-cell lymphoid malignancies. *Semin. Cancer Biol.* **2016**, *39*, 15–25. [CrossRef]
94. Wang, X.; Wang, L.; Dong, R.; Huang, K.; Wang, C.; Gu, J.; Luo, H.; Liu, K.; Wu, J.; Sun, H.; et al. Luteolin ameliorates LPS-induced acute liver injury by inhibiting TXNIP-NLRP3 inflammasome in mice. *Phytomedicine* **2021**, *87*, 153586. [CrossRef]
95. Wang, D.; Gao, Q.; Zhao, G.; Kan, Z.; Wang, X.; Wang, H.; Huang, J.; Wang, T.; Qian, F.; Ho, C.T.; et al. Protective Effect and Mechanism of Theanine on Lipopolysaccharide-Induced Inflammation and Acute Liver Injury in Mice. *J. Agric. Food Chem.* **2018**, *66*, 7674–7683. [CrossRef]

96. Gao, Z.; Zhang, C.; Tian, C.; Ren, Z.; Song, X.; Wang, X.; Xu, N.; Jing, H.; Li, S.; Liu, W.; et al. Characterization, antioxidation, anti-inflammation and renoprotection effects of selenized mycelia polysaccharides from Oudemansiella radicata. *Carbohydr. Polym.* **2018**, *181*, 1224–1234. [CrossRef]
97. Miao, F.; Geng, S.; Ning, D. Hydroxytyrosol ameliorates LPS-induced acute liver injury (ALI) in mice by modulating the balance between M1/M2 phenotype macrophage and inhibiting TLR4/NF-κB activation. *J. Funct. Foods* **2023**, *102*, 105455. [CrossRef]
98. Hu, B.; Liu, Q.; Jiang, Y.; Huang, Y.; Ji, H.; Zhang, J.; Wang, X.; Shen, X.C.; Chen, H. NIR-II Fluorescence/Photoacoustic Dual Ratiometric Probes with Unique Recognition Site for Quantitatively Visualizing H_2S_2 in Vivo. *Angew. Chem. Int. Engl.* **2025**, *64*, e202418378. [CrossRef]
99. He, Z.; Qiu, Z.; Liao, L.; Zhang, C.; Hu, S.; Zhao, S. Design and synthesis of photoacoustic probe for in situ imaging of hydrogen polysulfides in organs in vivo. *Sens. Actuators B Chem.* **2023**, *381*, 133423. [CrossRef]
100. Tang, Y.; Peng, J.; Zhang, Q.; Song, S.; Lin, W. A new NIR emission mitochondrial targetable fluorescent probe and its application in detecting viscosity changes in mouse liver and kidney injury. *Talanta* **2022**, *249*, 123647. [CrossRef]
101. Ouyang, J.; Hong, H.; Shen, C.; Zhao, Y.; Ouyang, C.; Dong, L.; Zhu, J.; Guo, Z.; Zeng, K.; Chen, J.; et al. A novel fluorescent probe for the detection of nitric oxide in vitro and in vivo. *Free Radic. Biol. Med.* **2008**, *45*, 1426–1436. [CrossRef] [PubMed]
102. Bian, C.; Liu, M.; Cheng, J.; Yang, L.; Li, Z.; Yu, M. Dual-Functional Fluorescent Probe in the Diagnosis of Liver Injury and the Evaluation of Drug Therapy with Double Signal Amplification. *Chem. Biomed. Imaging* **2024**, *2*, 156–164. [CrossRef] [PubMed]
103. Tang, H.; Qiang, X.; Gao, Y.; Teng, H.; Chen, X.; Zhang, Y.; Tian, J.; Qin, B.; Guo, Y. Real-time tracking and dual-mode imaging of hypochlorous acid in vivo by a small-sized fluorescence probe. *Dye. Pigment.* **2021**, *188*, 109219. [CrossRef]
104. Pan, Y.; Yang, Q.; Xu, H.; Yuan, Z.; Xu, H. Screening and optimization of a water-soluble near-infrared fluorescent probe for drug-induced liver injury monitoring. *Anal. Chim. Acta* **2023**, *1276*, 341654. [CrossRef]
105. He, C.; Liu, Q.; Zhang, X.; Wang, L.; Fu, S.; Zhang, H.; Li, S.; Li, Q.; Chen, S.; Hou, P. Visualizing ClO- fluctuations in drug-induced liver injury and bacterium via a robust ratiometric fluorescent probe. *Spectrochim. Acta Part A Mol. Biomol. Spectrosc.* **2024**, *323*, 124944. [CrossRef]
106. Fan, G.; Wang, N.; Zhang, J.; Ji, X.; Qin, S.; Tao, Y.; Zhao, W. BODIPY-based near-infrared fluorescent probe for diagnosis drug-induced liver injury via imaging of HClO in cells and in vivo. *Dye. Pigment.* **2022**, *199*, 110073. [CrossRef]
107. Roy, B.; Shieh, M.; Takata, T.; Jung, M.; Das, E.; Xu, S.; Akaike, T.; Xian, M. Phototriggered Hydrogen Persulfide Donors via Hydrosulfide Radical Formation Enhancing the Reactive Sulfur Metabolome in Cells. *J. Am. Chem. Soc.* **2024**, *146*, 30502–30509. [CrossRef]
108. Jia, R.; Zhang, H.; Zhang, W.; Zhao, H.; Zha, C.; Liu, Y. Protective effects of tenuigenin on lipopolysaccharide and d-galactosamine-induced acute liver injury. *Microb. Pathog.* **2017**, *112*, 83–88. [CrossRef]
109. Galanos, C.; Freudenberg, M.A.; Reutter, W. Galactosamine-induced sensitization to the lethal effects of endotoxin. *Proc. Natl. Acad. Sci. USA* **1979**, *76*, 5939–5943. [CrossRef]
110. Ansari, M.A.; Raish, M.; Bin Jardan, Y.A.; Ahmad, A.; Shahid, M.; Ahmad, S.F.; Haq, N.; Khan, M.R.; Bakheet, S.A. Sinapic acid ameliorates D-galactosamine/lipopolysaccharide-induced fulminant hepatitis in rats: Role of nuclear factor erythroid-related factor 2/heme oxygenase-1 pathways. *World J. Gastroenterol.* **2021**, *27*, 592–608. [CrossRef]
111. Wang, W.; Zhang, Y.; Li, H.; Zhao, Y.; Cai, E.; Zhu, H.; Li, P.; Liu, J. Protective Effects of Sesquiterpenoids from the Root of Panax ginseng on Fulminant Liver Injury Induced by Lipopolysaccharide/d-Galactosamine. *J. Agric. Food Chem.* **2018**, *66*, 7758–7763. [CrossRef] [PubMed]
112. Zheng, X.F.; Hu, X.Y.; Ma, B.; Fang, H.; Zhang, F.; Mao, Y.F.; Yang, F.Y.; Xiao, S.C.; Xia, Z.F. Interleukin-35 Attenuates D-Galactosamine/Lipopolysaccharide-Induced Liver Injury via Enhancing Interleukin-10 Production in Kupffer Cells. *Front. Pharmacol.* **2018**, *9*, 959. [CrossRef] [PubMed]
113. Wang, X.; Wu, L.; Zhang, Q.; Li, L.; Xie, Y.; Wan, X.; Wu, H.; Xiang, Y. Methyl 3,4-dihydroxybenzoate protects against d-galN/LPS-induced acute liver injury by inhibiting inflammation and apoptosis in mice. *J. Pharm. Pharmacol.* **2019**, *71*, 1082–1088. [CrossRef] [PubMed]
114. Wen, J.; Lin, H.; Zhao, M.; Tao, L.; Yang, Y.; Xu, X.; Jia, A.; Zhang, J.; Weng, D. Piceatannol attenuates D-GalN/LPS-induced hepatoxicity in mice: Involvement of ER stress, inflammation and oxidative stress. *Int. Immunopharmacol.* **2018**, *64*, 131–139. [CrossRef]
115. Yang, S.; Kuang, G.; Zhang, L.; Wu, S.; Zhao, Z.; Wang, B.; Yin, X.; Gong, X.; Wan, J. Mangiferin Attenuates LPS/D-GalN-Induced Acute Liver Injury by Promoting HO-1 in Kupffer Cells. *Front. Immunol.* **2020**, *11*, 285. [CrossRef]
116. Ai, G.; Wu, X.; Dou, Y.; Huang, R.; Zhong, L.; Liu, Y.; Xian, Y.; Lin, Z.; Li, Y.; Su, Z.; et al. Oxyberberine, a novel HO-1 agonist, effectively ameliorates oxidative stress and inflammatory response in LPS/D-GalN induced acute liver injury mice via coactivating erythrocyte metabolism and Nrf2 signaling pathway. *Food Chem. Toxicol.* **2022**, *166*, 113215. [CrossRef]
117. Guo, P.; Zeng, M.; Liu, M.; Zhang, Y.; Jia, J.; Zhang, Z.; Liang, S.; Zheng, X.; Feng, W. Isolation of Calenduloside E from Achyranthes bidentata Blume and its effects on LPS/D-GalN-induced acute liver injury in mice by regulating the AMPK-SIRT3 signaling pathway. *Phytomedicine* **2024**, *125*, 155353. [CrossRef]

118. Zhu, X.-Y.; Yao, H.-W.; Fu, Y.-J.; Guo, X.-F.; Wang, H. Effect of substituents on Stokes shift of BODIPY and its application in designing bioimaging probes. *Anal. Chim. Acta* **2019**, *1048*, 194–203. [CrossRef]
119. Wang, F.; Yu, S.; Xu, Z.; Li, L.; Dang, Y.; Xu, X.; Luo, Y.; Cheng, Z.; Yu, H.; Zhang, W.; et al. Acid-Promoted D-A-D Type Far-Red Fluorescent Probe with High Photostability for Lysosomal Nitric Oxide Imaging. *Anal. Chem.* **2018**, *90*, 7953–7962. [CrossRef]
120. Lin, X.; Chen, Y.; Bao, L.; Wang, S.; Liu, K.; Qin, W.; Kong, F. A two-photon near-infrared fluorescent probe for imaging endogenous hypochlorite in cells, tissue and living mouse. *Dye. Pigment.* **2020**, *174*, 108113. [CrossRef]
121. Wang, X.; Wang, H.; Duan, J.; Sun, Q.; Zhang, C.; Xu, L.; Liu, Z. Phenothiazine-hemicyanine hybrid as a near-infrared fluorescent probe for ratiometric imaging of hypochlorite in vivo. *Sens. Actuators B Chem.* **2024**, *407*, 135453. [CrossRef]
122. Duan, C.; Won, M.; Verwilst, P.; Xu, J.; Kim, H.S.; Zeng, L.; Kim, J.S. In Vivo Imaging of Endogenously Produced HClO in Zebrafish and Mice Using a Bright, Photostable Ratiometric Fluorescent Probe. *Anal. Chem.* **2019**, *91*, 4172–4178. [CrossRef] [PubMed]
123. Ji, Y.; Xia, L.-J.; Chen, L.; Guo, X.-F.; Wang, H.; Zhang, H.-J. A novel BODIPY-based fluorescent probe for selective detection of hydrogen sulfide in living cells and tissues. *Talanta* **2018**, *181*, 104–111. [CrossRef] [PubMed]
124. Li, T.; Wang, L.; Lin, S.; Xu, X.; Liu, M.; Shen, S.; Yan, Z.; Mo, R. Rational Design and Bioimaging Applications of Highly Specific "Turn-On" Fluorescent Probe for Hypochlorite. *Bioconjugate Chem.* **2018**, *29*, 2838–2845. [CrossRef]
125. Huang, Y.; Yu, F.; Wang, J.; Chen, L. Near-Infrared Fluorescence Probe for in Situ Detection of Superoxide Anion and Hydrogen Polysulfides in Mitochondrial Oxidative Stress. *Anal. Chem.* **2016**, *88*, 4122–4129. [CrossRef]
126. Zhu, X.-Y.; Wu, H.; Guo, X.-F.; Wang, H. Novel BODIPY-based fluorescent probes with large Stokes shift for imaging hydrogen sulfide. *Dye. Pigment.* **2019**, *165*, 400–407. [CrossRef]

Disclaimer/Publisher's Note: The statements, opinions and data contained in all publications are solely those of the individual author(s) and contributor(s) and not of MDPI and/or the editor(s). MDPI and/or the editor(s) disclaim responsibility for any injury to people or property resulting from any ideas, methods, instructions or products referred to in the content.